SUPPRESSION OF MULTIPACTOR BREAKDOWN IN SATELLITE RECTANGULAR WAVEGUIDES USING DC MAGNETIC FIELD

BY

AKOMA, HENRY EZE CHIGOZIE

(M.ENG./SEET/2007/1872)

DEPARTMENT OF ELECTRICAL/COMPUTER ENGINEERING,
SCHOOL OF ENGINEERING AND ENGINEERING TECHNOLOGY,
FEDERAL UNIVERSITY OF TECHNOLOGY, MINNA,
NIGER STATE.

MARCH, 2010

SUPPRESSION OF MULTIPACTOR BREAKDOWN IN SATELLITE RECTANGULAR WAVEGUIDES USING DC MAGNETIC FIELD

BY

AKOMA, HENRY EZE CHIGOZIE

(M.ENG./SEET/2007/1872)

A THESIS SUBMITTED TO THE POSTGRADUATE SCHOOL,

FEDERAL UNIVERSITY OF TECHNOLOGY, MINNA, NIGER STATE,

IN PARTIAL FULFILMENT OF THE REQUIREMENT FOR THE AWARD OF

MASTER OF ENGINEERING (M.ENG.) DEGREE IN

COMMUNICATION ENGINEERING

MARCH, 2010

DECLARATION

I, Akoma, Henry E.C.A (M.ENG/SEET/2007/1872) declare that the work described in this research "Suppression of Multipactor Breakdown in Satellite Rectangular Waveguides using DC Magnetic Fields" represent my original work and has not been previously submitted to the university or similar institution for the purpose of award of similar or any other degree.

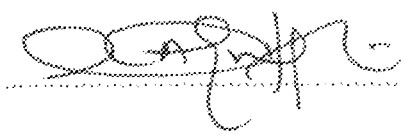

.....

Akoma, Henry E.C.A

Date

CERTIFICATION

This thesis titled: Suppression of multipactor breakdown in satellite rectangular waveguides using DC magnetic fields by Akoma, Henry Eze Chigozie (M.Eng/SEET/2007/1872) meets the regulations governing the award of the degree of Master of Engineering (M.Eng) of the Federal University of Technology, Minna and is approved for its contribution to scientific and literary presentation.

Engr. (Dr.) Y.A. Adediran
Supervisor

Signature & Date

Engr. A.G. Raji
Head of Department

(APRIL 9, 2010)
Signature & Date

Prof. O. Usifo
Dean, SEET

10/4/10
Signature & Date

Prof. S.L. Lamai
Dean, Postgraduate School

25/6/2010
Signature & Date

DEDICATION

Dedicated to my lovely wife, Kelechi aka Nkem, my son, Nnaemeka, who has brought joy to both our lives. To my parents, Rev. and Evang. (Mrs.) E.N Akoma, who made sacrifices to ensure I had a strong educational foundation.

ACKNOWLEDGEMENTS

I would like to express my profound gratitude and appreciation to my supervisor, Dr. Y.A. Adediran, for his meticulous, constructive and kindly guidance in the execution of this thesis. His passionate dedication to his academic responsibilities has been especially helpful in the realization of this research work. I would like to particularly appreciate the Vice-Chancellor, Professor M.S. Audu, the Dean, School of Engineering and Engineering Technology, Prof. O. Usifo, the Dean of PostGraduate School, Professor S.L. Lamai, the Head of Electrical and Computer Engineering Department, Engr. A.G. Raji and ali my lecturers for their respective contributions to the success of our program. I would like to further appreciate the Deputy Dean, School of Engineering and Engineering Technology, Dr. O. Chukwu, the Head of Mechanical Engineering Department, Prof. Khan, the Head of Agricultural Engineering, Dr. Balami, the Head of Civil Engineering, Dr. Sadiku, the Head of Chemical Engineering, Dr. Egharevbo and the entire Staff of School of Engineering.

Appreciation also goes to the team of project presentation panel, for the advice and observations made during the project presentation exercise.

Finally, I will love to acknowledge and appreciate the Management of the National Space Research and Development Agency (NASRDA) for providing the opportunity, financial and logistic support for the realization and attainment of the Masters degree in Engineering.

ABSTRACT

An important design consideration in systems utilizing hollow waveguides operating at low gas pressures and high RF power levels is the prevention or suppression of the multipactor breakdown phenomenon. Various suppression techniques currently employed include surface treatments (such as coating and sputtering) and surface geometry modification. However, surface treatment tends to degrade with time and surface geometry modification can be a complex operation. To complement the limitations of the suppression techniques stated above, the use of a DC magnetic field is proposed. The research investigates via a mathematical model the possibility of using a DC magnetic field to effect suppression of multipaction in a rectangular waveguide. The result of analysis of the model using MATLAB and MS Excel Spreadsheet applications suggests that a small magnitude DC magnetic field perpendicular to the electric field and in the wave propagation direction is effective in reducing multipaction. In addition, the result also suggests that the multipactor suppression technique is only viable for emission angles greater than 5° (i.e. $\Phi_e > 5^{\circ}$).

TABLE OF CONTENTS

CHAPTER TWO

CHAPTER THREE

LIST OF TABLES

LIST OF FIGURES

ABBREVIATIONS AND SYMBOLS

Abbreviations

DC	Direct Current
ECSS	European Cooperation for Space Standardization
NASA	National Aeronautics and Space Administration
RF	Radio Frequency
SEC	Secondary Electron Coefficient
SEE	Secondary Electron Emission
SEY	Secondary Electron Yield
SRF	Superconducting RF
SW	Standing Wave
TE	Transverse Electric
TW	Travelling Wave

Symbols

a	Wide dimensions of the waveguide
B	External magnetic field strength
b	Narrow dimensions of the waveguide
Ba_x	External magnetic field strength pointing in the x-axis
Ba_y	External magnetic field strength pointing in the y-axis
Ba_z	External magnetic field strength pointing in the z-axis
d	Parallel-plate separation distance
D_B	Deflection length
D_{BT}	Total Deflection length
e	Electron charge, -1.609×10^{-19} coulombs
E	Electric field
E_0	Electron threshold primary energy
E_1	First cross-over energy
E_2	Second cross-over energy
E_{max}	Primary impact energy for maximum δ
E_p	Primary electron impact energy
F	Force acting on an electron
F_m	Magnetic force acting on an electron
Fm_{ax}	Magnetic force acting on an electron in the x-axis
Fm_{ay}	Magnetic force acting on an electron in the y-axis
Fm_{az}	Magnetic force acting on an electron in the z-axis
k	Wave propagation constant
k_{se}	Smoothness factor for E_p

$k_{s\delta}$	Smoothness factor for δ
L_B	Distance over which the magnetic field is uniform, or solenoid length
m_e	Electron mass, 9.109×10^{-31} kilograms
N	Multipactor-odd number
P_f	Forward power
q	Positive charge, $+1.609 \times 10^{-19}$ coulombs
R	Radius of curvature due to deflection
t_o	Time of emission of initial electron
v	Velocity of electron
V	Accelerating voltage
V_0	Voltage amplitude
v_i	Electron impact speed
v_o	Electron emission speed
δ	True secondary electrons yield, or secondary electron coefficient
δ_{max}	Maximum true secondary electrons yield, or maximum secondary electron coefficient
ε	Specularly reflected electrons
η	Back-scattered electrons
μ_0	Permeability of vacuum
σ	Total Secondary Emission Coefficient
τ_{RF}	RF period
Φ_D	Angle of electron deflection
Φ_e	Angle of electron emission
Φ_i	Angle of electron impact
ω	RF angular velocity

CHAPTER ONE

1.0 INTRODUCTION

New generation telecommunication satellites are designed to cater for a constantly increasing number of users, requiring increasingly higher bit rates in the same frequency multiplex. The conjunction of both tendencies implies increasing power levels of RF equipment downstream from the power amplifiers to the output multiplexers. In this situation, different discharge phenomena may occur inside the microwave devices. The consequences may be damage on the equipment and link budget degradation.

In a vacuum environment, microwave discharges inside RF equipment may be caused by a primary electron accelerated by an electric RF field which hits a target surface causing an avalanche-like increase of electrons due to secondary emission. The phenomenon described is referred to as the Multipactor Effect. Under this vacuum and RF conditions, satellite microwave equipment such as waveguides, receivers, transmitters, diplexers, isolators and RF cables are prone to the Multipactor Effect which leads to damage and degradation in payload performance.

The Multipactor Effect becomes the dominant high-frequency breakdown mechanism for pressures at which the mean free path of a free electron exceeds the spacing between the broad walls of a rectangular waveguide operating in the dominant TE_{10} mode. The consequences of this breakdown include damage to equipment, link budget degradation, generation of excess heat which can lead to melting and cracking of components, increased noise generation, harmonic distortion and inter-modulation (when multiple frequency RF signals are applied), etc. An

important design consideration in a system utilizing hollow waveguides operating at low gas pressures and high RF power levels is the prevention or suppression of breakdown due to Multipactor Breakdown or Multipactor Effect or Secondary Electron Resonance.

Various suppression techniques are currently employed to reduce or possibly completely eliminate this phenomenon in satellite RF components. Chapter 2 of this thesis will detail some of these techniques, such as coating and surface geometry modification, and also the results of tests carried out using these techniques. Chapter 3 will focus on the technique concerned with in this thesis, which is suppression of Multipactor using DC Magnetic Fields.

1.1 The Theory of Multipactor Breakdown

A brief qualitative description of the Multipactor Breakdown starts with the assumption that there are a few free electrons present in a waveguide filled with gas at a low pressure. Under the influence of the applied RF electric field, practically every electron crosses the guide without colliding with a gas molecule. Upon striking the waveguide wall, secondary electrons are emitted with a certain statistical probability. For most materials the secondary emission yield (i.e. the total number of emitted secondary electrons per unit time divided by the total number of incident electrons per unit time) becomes greater than unity if the impact energy of the incident electrons is sufficiently high. If the transit time of an electron across the guide is equal to one-half the period of an RF cycle (or, more generally, any odd multiple of a half-period), then the number of electrons crossing back and forth in synchronism with the applied RF field increases very rapidly in avalanche fashion. As a result, further transmission of the Radio Frequency energy is disrupted (Wachowski, 1964).

1.1.1 Multipacting Process

The impact of an incident (primary) electron on a surface can lead to the emission of one or more secondary electrons from the material. Summarized by Becerra (2007), the emission process consists of three main steps:

1. The primary electron crosses the surface of interest and is attenuated by collisions within the material and absorbed.
2. The energy lost by the primary is transferred to electrons inside the material.
3. Some of the excited electrons move toward the surface and are attenuated on their way out by collisions. Those with enough energy to escape the material are secondary electrons and typically have much lower energies than the primary.

The European Cooperation for Space Standardization (ECSS, 2003) expands the typical multipaction event process as follows:

a. Free electrons exist within the RF field region of a component whose dimensions are small compared with the electron mean free path as a result of low pressure within the component.
b. The electric field within the component accelerates the free electrons towards an interior surface.
c. The electrons impact on the surface with appropriate energies to liberate more secondary emission electrons than were incident.
d. The alternating RF field reverses and accelerates the electrons away from surface, reducing the tendency for surface re-absorption of the low energy electrons.
e. Steps c. and d. together are such that the number of free electrons is increased by the interaction with the surfaces.

f. Moving under the influence of the applied RF electric field and the electron-electron mutual repulsion field, the electrons impact on an interior surface of the component after approximately n half-cycles of the RF field. The number n is the "order" or "mode" of the multipaction event and is almost always odd, signifying a multipaction event between two surfaces, such as in rectangular waveguides and the two conductors in a vacuum spaced coaxial cable.

g. Steps c. to f. are now repeated with an increase in the electron population at each impact causing exponential charge growth to occur until a limiting process, such as that caused by the electron-electron mutual repulsion, causes the electron cloud to saturate.

Secondary electron emission coefficient (SEE) has two components:

i. True secondary electrons coefficient, or simply, secondary electron coefficient, δ, and

ii. Back-scattered electrons coefficient, η

For each electron impacting a surface, an average number of true secondary electrons and back-scattered electrons are emitted. A fraction ε of the back-scattered electrons are specularly reflected electrons. Each coefficient depends both on the energy of the incident particle and its angle of incidence. The variation of the Total Secondary Emission Coefficient $\sigma = \delta + \varepsilon$ with incident particle energy E is unimodal, with a maximum of σ_{max} at $E = E_{max}$ and for many metals $\sigma > 1$ for a range of E as illustrated in Figure 1.1

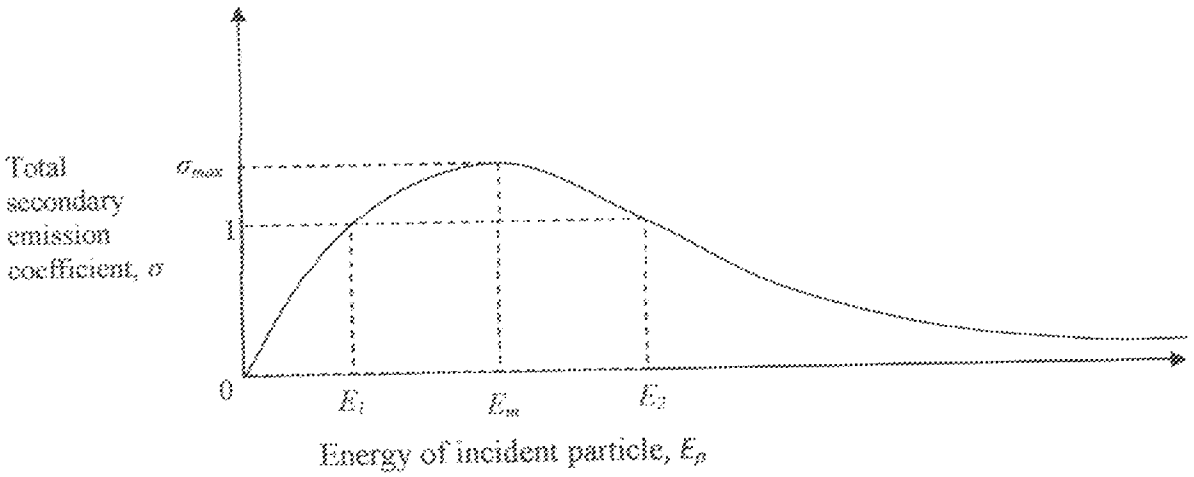

Fig. 1.1 : Total secondary electron emission as a function of energy of the incident electron [ECSS, 2003]

Gallagher (1979) explains that once initiated for whatever reason (field emission, ionization of residual gas, etc.) multipactor discharge consists of a thin electron cloud that is driven back-and-forth between the opposed surfaces (or gap) in response to the applied RF field. The exchange current in each half-cycle will increase to a limit set by the perveance of the gap, reaching steady state in a number of half-cycles set by the secondary emission coefficient. This perveance limit may be interpreted that as the electron density increases mutual repulsion causes some electrons to fall out of step with the applied field, thereby limiting the maximum electron density in the exchange cloud.

1.1.2 Secondary Emission Yield

The true secondary emission yield or secondary emission coefficient, δ or *SEY* or *SEC*, is defined as the mean number of secondary electrons emitted per incident primary. It is a function of the

energy and the angle of incidence of the primary electrons, and it must be greater than unity for electron multiplication to be possible for a statistically significant number of impacts.

For a given incidence angle, the secondary emission coefficient, δ, should vanish below a threshold primary energy E_0, increase at low energies (as primaries have some energy to transfer to the secondaries), reach a maximum, and decay at larger energies (as very fast primaries penetrate more deeply into the material and more of the excited electrons are stopped before they can reach the surface). This is indeed the case as has been shown experimentally, and secondary electron yield curves are usually identified by the maximum value δ_{max} and the primary energy at which the peak occurs, E_{max}. As seen from figure 1.2, the values for $E_1 < E_{max}$ and $E_2 > E_{max}$. E_1 and E_2 are the energies at which $\delta = 1$ and are known as the first and second crossover points.

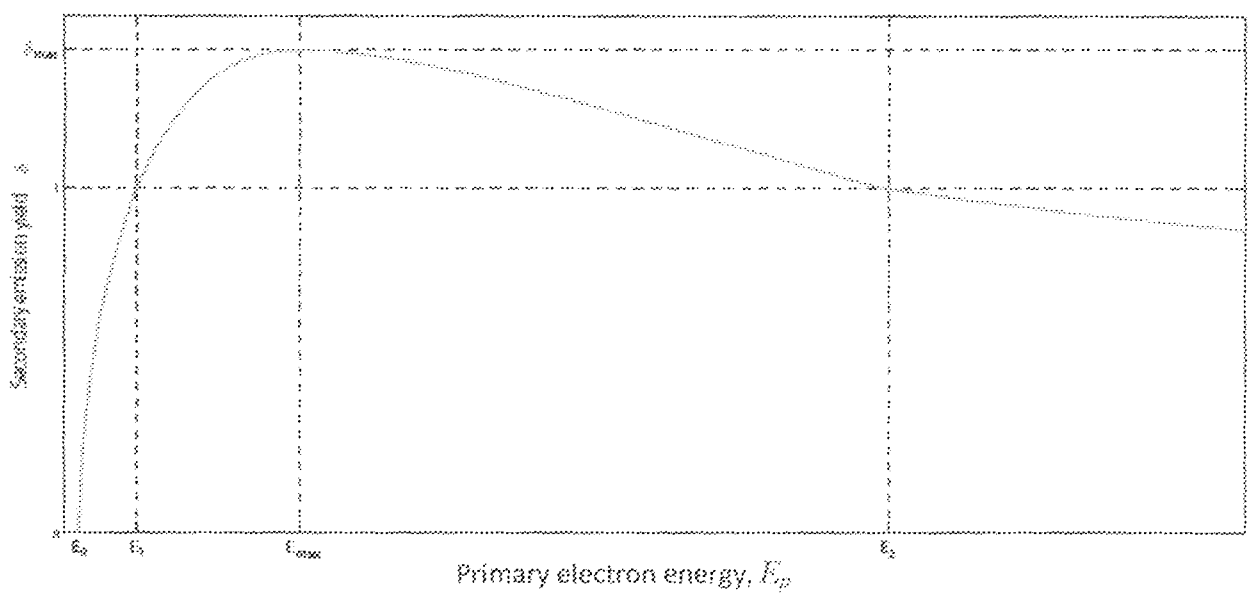

Fig 1.2 : Secondary emission yield curve and main characteristics at a fixed

Clearly, the primary energy, E_p, must lie between these two energies, E_1 and E_2, for there to be more secondary electrons emitted than primaries absorbed, which is crucial for a multipactor discharge to be sustainable.

1.1.3 Effect of Oblique Incidence

As illustrated in figure 1.3, when a primary electron is incident at an oblique angle to the surface, it is essentially attenuated in the same way as a primary incident normal to the interface, penetrating the same mean distance x_m into the material. However, the excited electrons are initially closer to the surface, so more of these can leave the material before being stopped on their way out. For an impact angle θ with respect to the normal, the mean depth changes by a factor $\cos\theta$, thus increasing the secondary yield. Such an increase has been observed experimentially (Kumar, 2006).

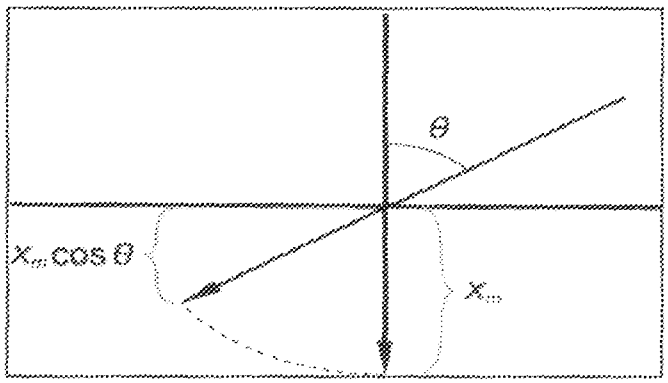

Fig. 1.3 : Effect of oblique incidence [Kumar, 2006]

Vaughan's empirical formulation concludes that both δ_{max} and E_{max} increase with incidence angle, while retaining the overall yield curve shape (Valfells *et al.*, 2000). Vaughan's formulas for oblique incidence corrections are

$$\delta = \delta(E_1) = \delta_{max}(we^{1-w})^k \tag{1.1}$$

$$E_{max}(\theta) = E_{max}(0)\left(1 + \frac{k_{sE}\theta^2}{\pi}\right) \tag{1.2}$$

$$\delta_{max}(\theta) = \delta_{max}(0)\left(1 + \frac{k_{s\delta}\theta^2}{2\pi}\right) \tag{1.3}$$

where δ_{max} is the maximum value of δ, $w = E_0/E_{max}$, E_{max} being the impact energy which yields δ_{max}, k=0.62 for w<1 and k>0.25 for w>1, k_{sE} and $k_{s\delta}$ are smoothness factors for E_0 and δ respectively, ranging from 0 to about 2.0, with a default value of 1.0 for typical surfaces. Low values correspond to deliberately roughened surfaces, while high ones are appropriate for very smooth and oxide-free surfaces. Figure 1.4 shows the effect of primary incidence at different angles on the secondary yield curves. Clearly, oblique incidence does not only raise δ_{max} and E_{max}, but it also decreases E_1 and increases E_2, thus widening the range for which $\delta > 1$ and making electron multiplication, critical for multipactor onset, more likely.

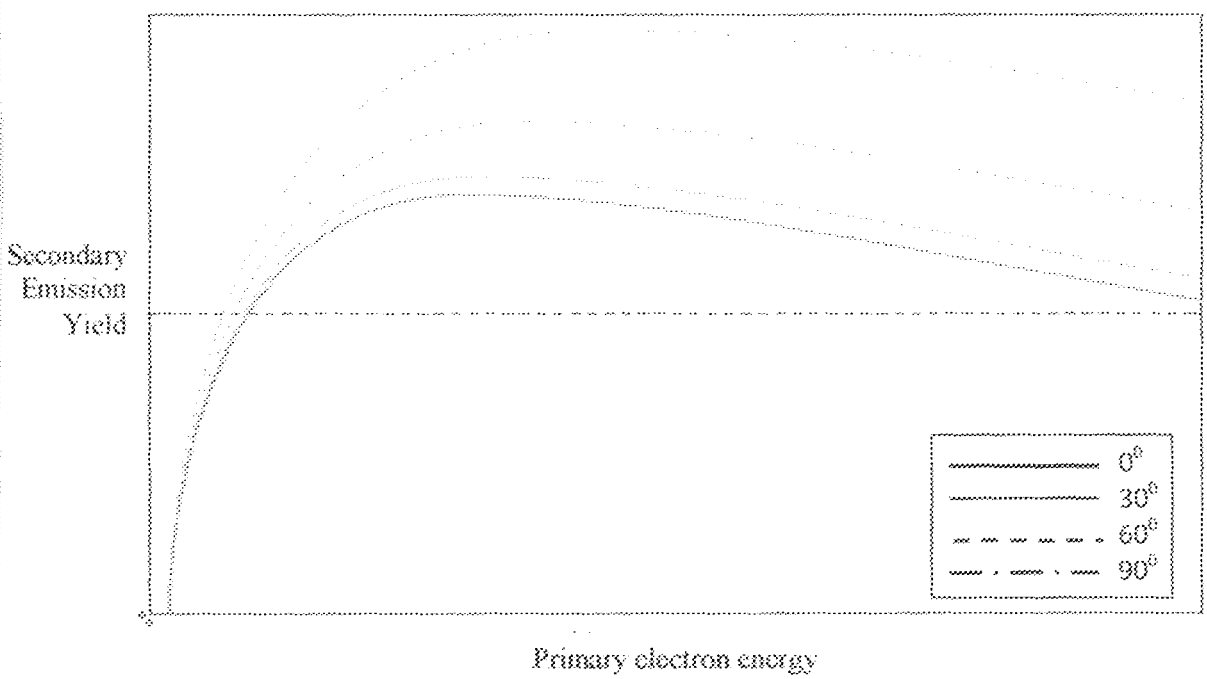

Fig. 1.4 : Vaughan's secondary emission yield curves for different angles of primary incidence [Becerra, 2007].

1.1.4 Effect of Surface Structure

Rough surfaces usually have smaller secondary emission yields than smoother ones, as can be seen from the yield parameters for different variations of carbon in Table 1.1. This is because peaks surrounding the point of emission of a secondary subtend a greater solid angle, thus increasing the likelihood of reabsorption of the electron by one of the peaks, especially for emission at the valleys of the surface. However, this is only valid in practice for very clean surfaces, since gases and impurities with higher secondary yields are adsorbed more strongly by rough surfaces, thus increasing the overall yield significantly if they are not removed. The change in δ due to adsorbed impurities can be up to approximately 0.5, with the effect being more important at lower primary energies, depending on the secondary yield characteristics of the substances (Becerra, 2007).

At the same time, the incidence angle is not properly defined for rough surfaces, so the effect of oblique incidence is essentially negligible for such cases. The smoothness factors in equations (1.2) and (1.3) reflect this, as a very rough surface corresponds to $k_{se} = k_{s\delta} = 0$ and no incidence angle effect.

Table 1.1 Secondary emission parameters for smooth surfaces of different variations of carbon at normal primary incidence [Becerra, 2007].

S/N	Carbon Type	δ_{max}	E_{max}	E_1 (eV)	E_2 (eV)
1	Soot	0.45	500	Not Available	Not Available
2	Graphite	1.02	300	250	350
3	Diamond	2.8	750	-	-

1.2 Statement of the Problem

Satellite-borne rectangular waveguides operate in a high vacuum space environment and also under high RF power. Both these conditions favour the initiation of the multipactor breakdown, a phenomenon which leads to damage and degradation in payload performance, and therefore limits greatly the output power of any communication satellite. Conventional multipactor suppression techniques such as surface treatments (coating and sputtering) and surface geometry modification have shown limitations in durability and production process respectively. To complement the limitations of the conventional suppression techniques mentioned, the use of a DC magnetic field is proposed. The research investigates via a mathematical model the possibility of using a DC magnetic field to effect suppression of multipaction in a satellite rectangular waveguide

1.3 Objectives of the Study

1. To model a complementary multipactor suppression technique different from the conventional surface treatment/coating and geometrical modification techniques in current usage.
2. To easily estimate specific waveguides geometries with given forward powers and frequencies.

1.4 Project Methodology

1.4.1 Modelling

The proposed multipactor suppression technique will be modeled using simple geometric and trigonometric quantities. The model will provide the relationship between the electron emission angle, deflection angle and impact angle. It will also show the relationship between the deflection angle, secondary electron yield and the DC magnetic field quantity.

1.4.2 Model Validation

The model will be validated using the standard engineering software tools MATLAB and MS Excel Spreadsheet. MATLAB will be used for graphical analysis while MS Excel Spreadsheet will be used for numerical analysis of the model.

1.5 Scope of the Study

This work will involve the review of previous research works on the subject, tests and results presented by individuals, institutions of higher learning and Space Agencies. A brief description of the Multipactor Theory will be provided. In addition, a review of conventional multipactor suppression techniques such as surface treatment/coating and geometry modification will be done. Finally the DC magnetic field suppression technique suggested by the work of Geng and Padamsee (Geng *et al.*, 1999) will be explored and a mathematical model designed in line with the technique.

The thesis is divided into five chapters.

1. Chapter One is an introduction to the concept of multipaction.
2. Chapter Two reviews previous works and materials on multipactor suppression.
3. Chapter Three provides the detailed model design for the DC Magnetic Field Multipactor Suppression Technique.
4. Chapter Four describes the validation of the multipactor suppression model using MATLAB and MS Excel Spreadsheet.
5. Chapter Five provides the thesis conclusion and recommendations.

CHAPTER 2

2.0 REVIEW OF RELEVANT LITERATURE

The first section of this chapter treats the most familiar scenario of multipactor without externally applied DC magnetic fields in the parallel-plate configurations. The second part reviews previous works on multipactor suppression (particularly surface treatment, geometry modification and application of an external DC magnetic field) and detection methods.

2.1 Unmagnetized Multipactor

Assuming vacuum conditions and ignoring all collective effects and negligible forces, the motion of electrons due to electromagnetic fields is governed by the Lorentz force:

$$F = -e(E + v * B) \tag{2.1}$$

where e is the elementary charge moving with a velocity v, E is a time-varying electric field and B is the magnetic field. Using the equation of motion, this force can be written as

$$F = m_e \frac{dv}{dt} \tag{2.2}$$

where m_e is the electron mass and $\frac{dv}{dt}$ represents the electron acceleration. Thus, combining equations (2.1) and (2.2) gives

$$\frac{dv}{dt} = -\frac{e}{m_e}(E + v * B) \tag{2.3}$$

For a rectangular waveguide, which is the transmission line geometry of interest, the amplitude of the electric field is c times that of the magnetic field, where c is the speed of light; so the magnetic force term can be neglected for non-relativistic electrons. Simulations and measurements in the configurations of interest show very few electrons with velocities above a few percent of c, so ignoring the magnetic force is generally an appropriate approach (Becerra, 2007). The problem is essentially reduced to one dimension, either by assuming that the electron is "average", meaning that it is emitted normal to the surface, or by simply ignoring any motion perpendicular to the electric field, since there are no significant transverse forces. The equation of motion is then solved for the initial conditions, namely the time of emission of the electron and its position and velocity in the direction of the field at that time. A second electron is assumed to be launched with similar initial conditions from the opposite electrode.

For electrons to contribute to a two-sided (between two metallic surfaces or two parallel plane surfaces, separated by a gap) multipactor discharge, two conditions must be satisfied (Becerra, 2007):

1. There must be synchronism between the impacts and the alternating field, so for the process to be repeated cyclically, the transit times of the forward and backward electrons, Δt_1 and Δt_2 respectively, have to add up to an integer number of RF periods. That is,

$$\Delta t_1 + \Delta t_2 = n T_{RF} = 2\pi n/\omega \tag{2.4}$$

where ω is the angular frequency of the RF signal.

2. For there to be electron multiplication in the gap, the product of the secondary electron coefficients at the impact energies (and incident angles if transverse motion is not ignored) must be greater than unity.

2.1.1 Parallel-Plate Multipactor (Two-Sided Multipactor)

Considering a single electron between two parallel plates at $x = 0$ and $x = d$ in an alternating field $E_x = -E_0 \sin \omega t$, and setting the time origin as the zero phase of the RF field, the equation of motion is given by

$$\frac{dv_x}{dt} = \frac{d^2x}{dt^2} = \frac{eE_0}{m_e} sin\omega t \tag{2.5}$$

The minus sign in the electric field is chosen such that the force is in the positive x direction for a small positive t. The equation can be solved analytically, provided the following initial conditions at the time of electron emission t_0 from one of the electrodes are satisfied:

$$x(t = t_0) = 0 \tag{2.6}$$

$$v_x(t = t_0) = v_0 \tag{2.7}$$

The velocity and position of the electrons are then found by integrating the equation of motion, taking the initial conditions into account (Becerra, 2007):

$$v_x(t \geq t_0) = v_0 + \frac{eE_0}{m_e\omega}(\cos \omega t_0 - \cos \omega t) \tag{2.8}$$

$$x(t \geq t_0) = v_0(t - t_0) + \frac{eE_0}{m_e\omega}(\sin \omega t_0 - \sin \omega t + (\omega t - \omega t_0) \cos \omega t_0) \tag{2.9}$$

Since the electric field in the parallel-plate geometry is independent of x, the synchronism condition for multipactor can be simplified by assuming that v_0 is the same for every electron,

since in that case the condition becomes that every electron's transit time has to be an odd integer number of RF half-periods. If this is satisfied for the first electron, the second electron automatically satisfies it since its motion would be subject to the same forces in the reverse direction. Similarly, assuming equal angles of incidence, it means that $\delta_1 = \delta_2$.

Making the assumption that v_0 is consistently the same for all electrons, the synchronism condition becomes $x(t = t_0 + N\pi/\omega;\ N \text{ is odd}) = d$. This reduces equation (2.9) to

$$d = \frac{N\pi v_0}{\omega} + \frac{eE_0}{m_e\omega^2}(2\sin\omega t_0 + N\pi\cos\omega t_0) \tag{2.10}$$

So the voltage amplitude $V_0 \equiv E_0{*}d$ is given by

$$V_0 = \frac{m_e}{e}\frac{\omega d(\omega d - N\pi v_0)}{(2\sin\omega t_0 + N\pi\cos(\omega t_0))} \tag{2.11}$$

Given v_0, the minimum V_0 satisfying the synchronism condition is such that the denominator is maximized, which happens when $\omega t_0 = \arctan(2/N\pi)$, giving

$$V_{0,min} = \frac{m_e}{e}\frac{\omega d|\omega d - N\pi v_0|}{(4+N^2\pi^2)^{1/2}} \tag{2.12}$$

which is thus the lower boundary for the onset voltage of a multipactor discharge of the mode characterized by the given N, provided v_0 is such that the condition of electron multiplication upon impact is also satisfied. The upper boundary for the onset voltage can also be obtained by using the maximum negative value of t_0 such that the emission velocity v_0 is just enough for the electron to overcome the initially retarding field, though this cannot be expressed explicitly in a general closed-form equation. The impact velocity, obtained by imposing the synchronism condition, is

$$v_f \equiv v_x\left(t = t_0 + \frac{N\pi}{\omega}\right) = v_0 + \frac{2eE_0}{m_e\omega}\cos\omega t_0 \tag{2.13}$$

from which the impact energy, using the secondary emission notation, can be calculated as $E_p = \frac{1}{2}m_e v_f{}^2$. The secondary emission yield at this energy for the angle of incidence of interest must then be greater than unity for multiplication to be possible over a large number of cycles, such that electrons with the given conditions can contribute to the development of multipactor discharges. Evidently, out of the electrons satisfying the synchronism condition, those emitted at $\omega t_0 \pmod{2\pi} \approx 0$ have greater impact energies and, for materials with a very large second crossover energy, are more likely to satisfy the multiplication condition. This leads to phase focusing or phase selection, such that the electron population over many cycles is restricted to the phases that satisfy the said condition and concentrates around the phases that lead to impact energies around E_{max}. The phase range increases with greater electric field amplitude, as more electrons can reach impact energies high enough for effective multiplication.

2.2 Review of Previous Works

Multipactor prevention techniques usually fall in one of the following categories: geometric fixes, pressurization, amplitude modulation of main carrier, DC biasing, and surface treatments. The first is usually the most effective, consisting of changing the geometry of multipactor-susceptible sections such that it is unfavorable for resonance conditions. DC biasing involves suppressing electron motion across a gap by applying a large DC electric field bias between the electrodes. However, both of these are often subject to other engineering constraints, and become considerably more complicated in certain systems in the presence of a large magnetic field.

Surface treatments, designed to lower the secondary emission yield of the surfaces, are less susceptible to these constraints, but can degrade over time.

2.2.1 Suppression of Secondary Electron Emission from the Electrodes of Multistage Collectors

Dayton (1997) reviewed more than 20 years of research conducted at NASA Lewis Research Centre on the suppression of secondary electron emission (SEE) for the enhancement of the efficiency of vacuum electron devices with multistage depressed collectors. He stated that typically secondary electrons are emitted in a spectrum of energies ranging from near zero up to the energy of the primary electron. The distribution of electrons within this energy spectrum is a function of the energy and angle of incidence of the primary electrons as well as the material and surface morphology of the target. The research was primarily focused on the aspect of material and surface morphology of different targets.

The paper included a description of measurement techniques and data from measurements of secondary electron emissions (SEE) on a variety of materials of engineering interest. The technique of ion sputtering (or ion texturing) was used to provide surface coating for the target materials under test and significant secondary electron yield reduction was observed when compared to the untreated materials. Results of this research work are shown in Table 2.1.

A drawback of the ion sputtering technique used is its complexity especially when compared to the simple sublimation technique used in the deposition of Titanium on target surfaces (Primdahl *et al.*, 1992). In the course of the work a very low secondary electron yield was achieved for ion textured graphite, and, in a parallel line of research, the highest yield was obtained for chemical vapor deposited thin diamond films.

Table 2.1 Secondary Electron Emission Characteristics of Candidate MDC Electrode Materials at 500 eV Primary Beam Energy, Normal Incidence [Dayton, 1997]

S/N	Material	Secondary Electron Emission Ratio
1	Copper (untreated)	0.94
2	Copper (sooted)	0.33
3	Textured Carbon on Copper	0.26
4	Pyrolyzed Carbon on Copper	0.41
5	Ta-Seeded Ion-Textured Copper	0.39
6	304SS-Seeded Ion-Textured Copper	0.34
7	AB Surface (Untreated)	0.82
8	AB Surface (Ion-Textured)	0.30
9	Carbon Surface (Untreated)	0.49
10	Carbon Surface (Ion-Textured)	0.22
11	POCO Graphite (Untreated)	0.64
12	POCO Graphite (Particle-Blasted)	0.53
13	POCO Graphite (Ion-Textured)	0.20
14	Ta-Seeded Ion-Textured Titanium	0.40
15	Ti Carbon/Copper	0.60
16	Ta	0.90
17	Beryllium	0.70

2.2.2 Measurement of Multipacting Currents of Metal Surfaces in RF Fields

Proch *et al.* (1996) presented data of the systematic measurements of RF multipacting current between two electrodes of a specially designed coaxial resonator. Technical surfaces (Cu, plated Cu on stainless steel, Al, stainless steel) were investigated before and after surface treatments such as chemical cleaning, baking and Ti coating. After each measurement the samples were slightly chemically polished so that a new surface was prepared for the next measurement. Some Cu samples were coated with Ti (sputter technique), one sample was coated with TiN (thermal evaporation). Four stainless steel samples were electroplated with Cu. Four samples (2 Cu, 2 Ti on Cu) were stored in a plastic bag (filled with dry N_2) for one week. Table 2.2 summarizes the measured results.

All samples showed multipacting of at least first order. They differed in magnitude of multipacting current and in processing time. Al samples showed the worst behavior. Coating of Cu with Ti reduces the processing time to about 45%. A Ti coating of Al had a substantial improvement because of the strong multipacting behavior of the bare Al. After coating with Ti, samples from Cu and Al behave the same. Electroplated Cu on stainless steel is somewhat worse than pure copper before heat treatment. One interesting result is the dramatic deterioration of Cu and Ti coated Cu samples after storage in a plastic (PE) bag. The mechanism is not understood. One speculation is that some lubricant in the PE foil penetrates to the metal surface of the sample. Nevertheless, the common practice to store or transport RF components in plastic bags should be avoided, if multipacting is of concern.

Table 2.2 Results of the multipacting measurements (*N*: number of measurements; *I*: multipacting current; *E*1, *E*2: electric field gradient at onset and stop of multipacting current respectively (Proch et al, 1996).

S/N	Material	*N*	*I* (mA)	*E1* (KV/m)	*E2* (KV/m)
1	Copper	18	2.92	132.1	188.4
2	Copper (heated at 400°C)	2	3.52	145.8	231.4
3	Cu, stored one week in PE bag	2	3.30	82.5; 139.0	108.9;192.8
4	Titanium on Copper	5	3.03	139.9	184.5
5	TiN on Copper	1	3.00	129.3	170.7
6	Titanium on Aluminium	2	2.88	141.8	183.4
7	Cu Ti, stored one week in PE bag	2	3.21	51.1; 123.6	68.1; 190.0
8	Aluminium	7	4.30	54.7	69.4
9	Stainless Steel	18	3.37	69.3;128.8	87.7; 147.6
10	Copper electrochemically plated on Stainless Steel	7	3.33	132.7	183.8

2.2.3 Suppression of the Effective Secondary Emission Yield for a Grooved Metal Surface

Stupakov *et al.* (2004) in the paper showed that a grooved surface can have an effective secondary emission yield (SEY) smaller than a flat one. Two different geometries of grooves, triangular and rectangular, were studied. The effect of strong magnetic field on SEY suppression was also considered. The analysis was based on a computer simulation which tracked orbits of

the secondary electrons and used a detailed model for the energy and angular distribution of the secondaries.

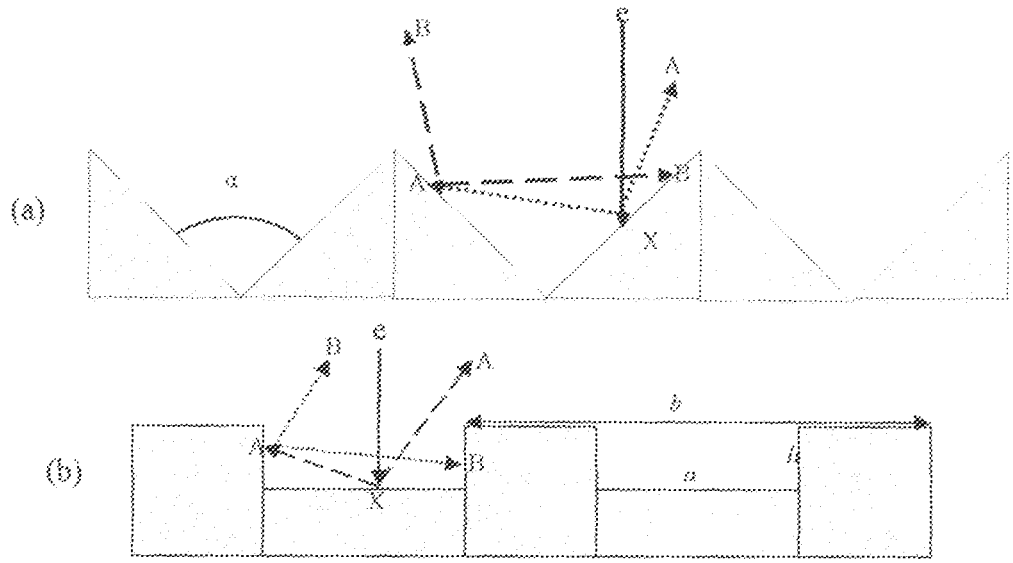

Fig. 2.1: Triangular (a) and rectangular (b) grooves on the surface. Triangular grooves are characterized by the angle α. Rectangular grooves have a period *b*, width *a* and depth *h*.

The triangular grooves were characterized with angle α and the rectangular grooves by the period *b*, width *a* and depth *h* as shown in figure 2.1. An initial electron, whose trajectory is as shown in the figure, hits the surface at point X and produces secondary electrons shown as lines A. Depending on the emission angle, some of the secondary electrons can escape the groove and move away from the surface. Other secondary electrons would hit an inner side of the groove. With some probability they will be absorbed, or they can generate other secondary electrons (which are referred to as the second generation secondaries) whose trajectories are shown as lines B. The process may repeat several times until the energy of higher generations of the secondaries becomes too low and they are eventually absorbed by the surface.

Stupakov *et al.* (2004) stated that an initial electron that travels perpendicular to the horizontal plane in figure 2.1 would hit the surface of the groove at an angle $(\pi-\alpha)/2$ relative to the normal to the surface. Since *SEY* is typically proportional to the incidence angle, this means that there is a higher probability of the number of first generation secondaries being smaller than that of a flat surface. This probability was calculated and simulated using the subroutine POSINST. The results of this simulation show that the magnitude of suppression of the *SEY* depended on the angle of the triangular grooves and on the aspect ratio of rectangular grooves as shown in *Figure*s. 2.2 and 2.3.

From *Figure*. 2.2, the top curve gives the reference value of secondary electron yield, $\delta(E)$, (where E is the incident energy of the electron) for a flat surface (without grooves) for normal incidence. The lowest curve is the effective *SEY* with grooves when only first generation of secondaries is taken into account (that is each secondary electron is assumed to disappear when it hits a wall). The middle dots (middle curve) show the result of simulation with two generations of secondaries taken into account (second generation secondary electrons do not produce secondaries when they hit the wall). As it is shown in the figure, the maximum effective *SEY* decreases to a value of about 1.3 in this case. Simulations also showed that smaller angles result in a stronger suppression of the emission.

Figure. 2.3 shows result of the simulation for rectangular grooves assuming $a = (2/3)*b$. The rough lines correspond to different aspect ratios of the rectangular grooves; the bottom line is for $h/a = 2$, and the middle one corresponds to $h/a = 1$, while the top curve corresponds to a

reference flat surface. As in the case of triangular shapes, deeper grooves show higher suppression of secondary emission.

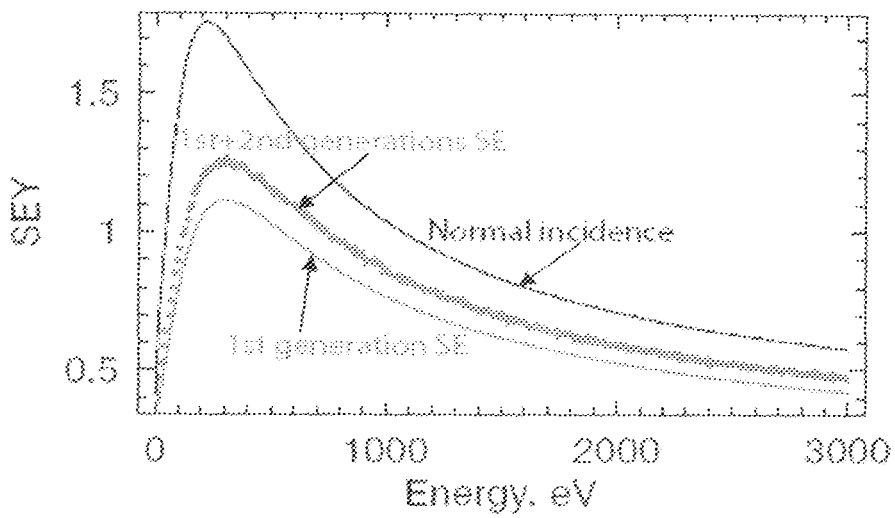

Fig. 2.2: SEY as a function of incident energy for triangular grooves with $\alpha = 60^0$ [Stupakov et al, 2004].

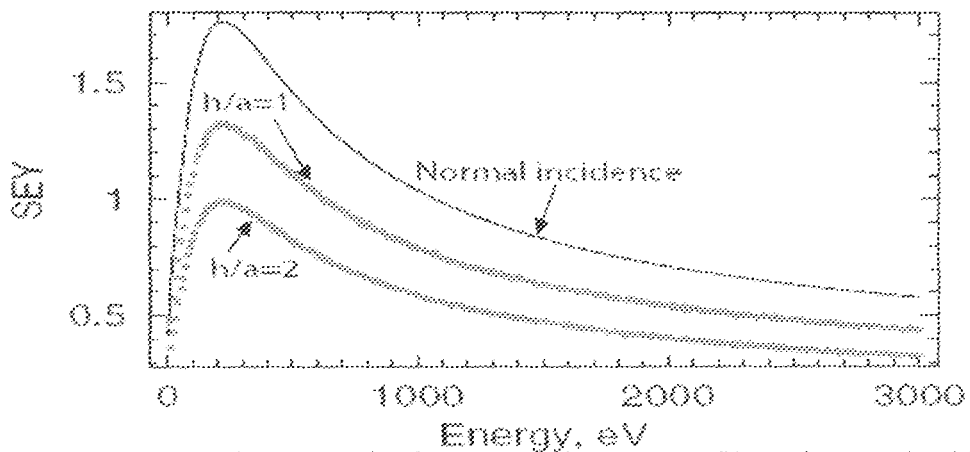

Fig. 2.3:Simulation results for rectangular grooves [Stupakov et al, 2004]

2.2.4 Multipactor Studies of Rectangular Waveguides

Goudket *et al.* (2003) presented the results of experimental and numerical studies of multipactor in rectangular waveguide geometries. A new section of rectangular waveguide similar to the input coupler of the CESR-type SRF cavities was designed to experimentally verify various multipacting suppression methods.

Simulations were performed to assess the effectiveness of grooves for suppressing multipactor. The grooves were cut out of a waveguide broad wall, to a width and depth of 1cm. To improve the description of the fields in the vicinity of the grooves, the mesh density was increased so that the groove width was covered by a minimum of five cells. It was apparent during the simulation that the grooves trapped electrons in a low field region, where they stayed until they were absorbed by the walls or leave the groove. The effectiveness of this multipacting suppression method appeared to depend on the number of grooves cut into the walls as well as their size. It also appeared that a ridge of the same dimensions as the groove had a similar effect.

2.2.5 Electron Multipacting in CESR Type Rectangular Waveguide Couplers

Geng *et al.* (2004) discussed the results from an experimental waveguide section, as well as simulations from a model of electron multipacting using the MAGIC PIC code. Tests were carried out on a new waveguide section that included enhanced diagnostics and the possibility of changing surface materials and temperature. Those tests evaluated grooves, ridges and surface coatings, including a Titanium Nitride (TiN) coating and a Titanium Zirconium Vanadium Non Evaporated Getter (TiZrV NEG) coating, as methods of multipactor suppression. Multipacting current was measured using electron probes placed at strategic points on the waveguide plate.

The conclusion after those tests remains that the most effective method to achieve complete multipactor suppression remains the application of a static magnetic bias, parallel to the wave propagation direction.

2.2.6 Multipactor-Inhibited Waveguide Geometry

Chojnacki (2000) presented the equations used to design a multipactor simulation code and the results of simulation studies of a wedge-shaped hollow waveguide geometry that showed promise of being far less susceptible to multipactor resonances than standard coax and hollow rectangular waveguides. Following a previous work on multipactor done by which accomplished suppression by implementation of a rounded superconducting RF (SRF) cavity profile, Chojnacki explains that since both rectangular and coaxial waveguide multipactor trajectories remain well aligned with the respective mode's electric field, a resonance-disrupting effect may be provided by altering the waveguide cross section so as to force curvature on the electric field. This could disallow trajectories from traversing repeatable paths and even guide electrons to regions of zero electric field. One such unconventional waveguide cross section is illustrated in *Figure*. 2.4. A rectangular waveguide is altered to have the broad walls nonparallel and the sidewalls as circular arcs to facilitate analysis. This "wedgeguide" has a lowest-cutoff mode similar to the rectangular TE_{10}.

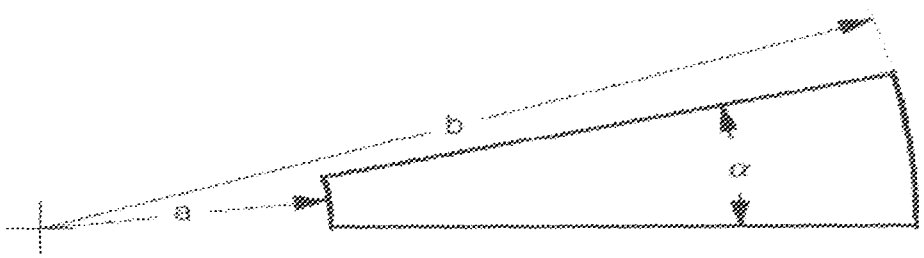

Fig. 2.4 : Wedge-shaped cross section of a hollow waveguide (Chojnacki, 2000).

The wedgeguide dimensions were taken as a modification to the CESR 10.2 cm * 43.2 cm rectangular waveguide where one sidewall is effectively reduced to a 5.1 cm height and the other increased to 15.2 cm by having dimensions of a = 21.6 cm, b = 64.8 cm, α =13.2° (as shown in *Figure*. 2.4), and again driven at 500 MHz.

Running simulations over comprehensive ranges of RF power, launch phase, and launch position in wedgeguide revealed three characteristics of electron trajectories.

I. The great majority of trajectories alternately impact on the broad walls and quickly become anti-resonant with the RF. After a dozen or so impacts, the accumulated secondaries perform successive low energy impacts, and secondary multiplication quickly decays to negligible values.

II. Trajectories have a migration bias toward the larger radius sidewall due to the E field curvature. Trajectories that survive anti-resonant conditions well enough to maintain a significant secondary multiplication typically migrate to this wall. There, the vanishing electric and finite magnetic fields allow only successive cyclic low energy impacts that quickly damp secondary multiplication to negligible levels, analogous to trajectories displaced from the midline in normal rectangular waveguides.

III. The outward radial migration due to the E field curvature opposes the net inward radial $v_\theta * B_z$ force that occurs at radii less than the peak of the E field. For a range of trajectory radii there are specific RF power levels at which these opposing forces almost balance, and the electrons can remain close to resonance. Fortunately, the force balance is not constant along the trajectory

nor on average, and the electrons eventually become anti-resonant and/or migrate to a sidewall, in either case, ultimately experiencing successive low energy impacts that quickly damp secondary multiplication to negligible levels. Figure 2.5 shows the trajectory of an electron launched at a radius of 32 cm in wedgeguide and temporarily experiencing almost balanced transverse forces.

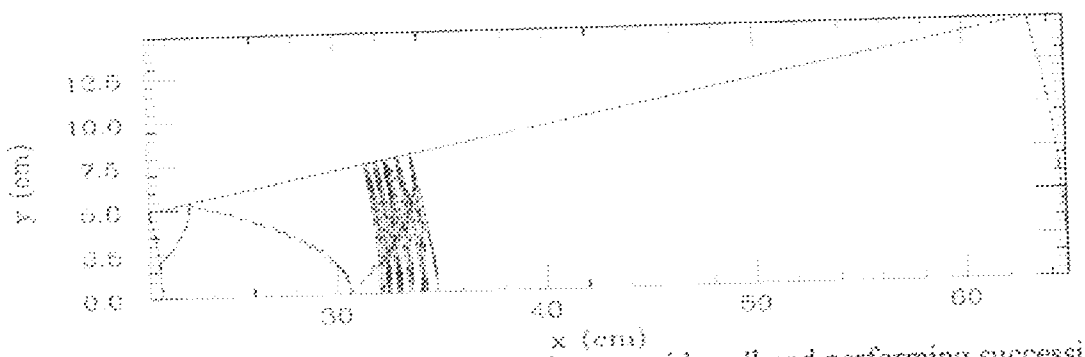

Fig. 2.5: Trajectory of an electron migrating to a sidewall and performing successive low energy impacts to reduce secondary multiplication [Chojnacki, 2000].

In conclusion, Chojnacki states that electron trajectory simulations show the "wedgeguide" waveguide geometry to be promising in having greatly reduced multipactor susceptibility, no resonances being found after simulating a multitude of cases of RF power, launch phase, and launch position.

2.2.7 Multipacting Characteristics of a Rectangular Waveguide

Geng *et al.* (1999) carried out investigations into the multipacting characteristics of the rectangular waveguide used for CESR-III Superconducting RF (SRF) system by using a newly developed 3-D computer code. Multipacting bands were identified for different operating modes, such as standing wave (SW) mode, traveling wave (TW) mode and the so-called mixed wave

mode (TW mixed with SW). A comparison between the simulation results and the experimental observations for the installed CESR-III SRF systems was made. Measures to suppress multipactor were explored. The simulation results suggested that an external DC magnetic field of a few Gauss of amplitude in the wave propagation direction would be very effective in disturbing the trajectories.

2.2.8 Effects of an External Magnetic Field, and of Oblique RF Electric Fields on Multipactor Discharge on a Dielectric

Valfells *et al.* (2000) analyzed, separately, the effects of an external magnetic field, the RF magnetic field, and an oblique RF electric field, on multipactor discharge on a dielectric. Using Monte Carlo simulation, they obtained the susceptibility diagram in terms of the magnetic field, the RF electric field, and the dc charging field for various dielectric materials. It was found that a magnetic field parallel to either the RF electric field or the DC electric field does not qualitatively change the susceptibility diagram. However, an external magnetic field perpendicular to both the RF electric field and the DC electric field can significantly affect the susceptibility diagram. Thus, oriented magnetic fields lower the upper susceptibility bound, via resonance effect, when the magnetic field strength is approximately equal to B_{res}=0.036f (GHz), where B_{res} is measured in Tesla and f is the RF frequency. Both the lower and upper susceptibility boundaries may be raised significantly by a large external magnetic field, B>>B_{res}. Susceptibility to single surface multipactor is greatest when the RF electric field is nearly parallel to the dielectric, but is dramatically decreased for angles of obliqueness greater than approximately 5°–10°. The RF magnetic field does not affect the lower boundary, but may extend the upper boundary greatly.

2.2.9 Multipaction for SRF Cavities for Accelerator Driven Sub-Critical System (ADSS)

Ghatak *et al.* (2008) gave a presentation on their work on the simulation of multipaction in a 700 MHz elliptical SRF cavity. The cavity design was optimized using SUPERFISH. Then the electromagnetic field was recomputed with FEMLAB, a package that uses the finite element method, to obtain a more accurate field-mapping, and to make the field values available for computation of multipaction. In the multipacting subroutine, electrons were assumed to be released into the system from various points with different initial parameters. The electron trajectories were tracked until they hit the cavity surface. Leap-frog scheme was used to solve the Lorentz force equation for primary electrons, as it is easy to use and is accurate up to the second order. The position, velocity, phase and kinetic energy of primary electrons at each time step are calculated and stored. An interpolation function is used to calculate secondary emission yield (SEY) at different impact energies. With the emission of secondary electrons, their trajectories too were tracked along with primary electrons, in order to identify parameters responsible for multipaction. By repeating this process for large number of electrons, the multipacting trajectories and field levels were identified.

For the verification of the developed code, a TESLA cavity was analyzed and the trajectories verified with those reported to have been obtained from Multipac, a simulation software toolbox for analyzing electron multipacting in axi-symmetric structures. With the developed code, the authors were able to conclude that the designed cavity was likely to be multipacting-prone. It was also possible to identify the multipacting sites and field levels, as well as the order and type of multipacting expected. As a next step, the requisite cavity was to be redesigned to make it

multipacting-free as far as possible. This code may also be extended for 3 dimensional cavity structures and other RF components like couplers, windows, etc.

2.2.10 Suppression of Multipacting in Rectangular Coupler Waveguides

Dykes *et al.* (2003) discussed the results of two experimented methods that could be used to suppress multipacting in a rectangular coupler waveguide:

i. the slotted waveguide method, and

ii. the DC magnetic bias method

The slotted waveguide method calls for opening slots on the broad walls in the wave propagation direction that perturb the resonance and trap multipacting electrons. Experimental observation showed that when the slotted waveguide featured with one slot (5 mm wide by 5 - 10 mm deep) along the centre line of a broad wall, multipacting current was reduced by a factor of 2 to 7 for the power range of 0 - 500 kW in traveling wave mode. Observation and imaging of activities inside the waveguide space was made through view ports installed on the E-bends located on both sides of the test waveguide. In the waveguide space corresponding to the slot, a dark region was visible against the whitish-blue background, which was due to discharge of gas molecules desorbed by multipacting electrons. This observation not only confirmed the multipacting suppression effect of the slot, but also revealed that multipacting developed across broad walls over almost the entire width of the waveguide. It was thus concluded that, to achieve a complete multipacting suppression with the slotted waveguide method, multiple slots were needed on both broad walls.

The DC magnetic bias method utilized a solenoid coil wrapped around the waveguide to generate a mild DC magnetic field in the waveguide space that bends the trajectory of multipacting electrons. Complete multipacting suppression was realized with the DC magnetic bias method. It was anticipated that the DC magnetic bias method could also be applied to coaxial coupler waveguides, because a solenoid magnetic field provides similar trajectory bending for multipacting electrons of the one-sided outer conductor multipacting. An advantage of the DC magnetic bias method is that coupler waveguide segments having different dimensions can be fitted with different solenoid coils, each proving an optimal biasing field.

2.2.11 Secondary Electron Yield Variation with Surface Treatment

Baglin *et al.* (2000) discussed the results obtained after application of various surface treatment methods on technical surfaces (such as copper, niobium and aluminium) with respect to *SEY* reduction. Treatment methods employed on the technical surfaces included

i. modification of the surface composition, and

ii. modification of the surface roughness

Modification of the surface composition was accomplished by the bombardment of technical surfaces with argon ion. Argon ion glow discharge treatment is a powerful way to modify surfaces. By changing the argon compound used during this treatment, it was possible to produce various surface layers lowering permanently the *SEY* even after 24 hours exposure to air. Argon compounds used included AO_2GD (argon + 10% oxygen) and N_2GD (argon + nitrogen).

Another possible way to lower the *SEY* was to change the surface roughness. This causes indirectly a reduction of the emissivity of the surface since the solid angle for electrons to escape without further interaction with the surface can be significantly decreased. This modification was produced by the deposition of a strongly dendritic layer. The creation of a strong dendritic surface on a small copper sample produced a surface which had a *SEY* lower than 1, even after exposure to air.

In-depth review of materials on the multipactor phenomena and its attendant negative effects on RF communication components and equipment, particularly the ones on a space-borne satellite, has been done. Also, possible suppression techniques (suggested and adopted) have been studied. While surface treatment (coating, sputtering, etc) of satellite RF components minimizes the onset of the multipactor, it has been noted that treatments such as coating tend to degrade with time. Dykes *et al.* (2003) experimental research was able to show the mathematical relationship between the DC magnetic bias field to fully suppress multipacting and the rectangular waveguide geometry. However, the work did not indicate for the said geometry the amount of deflection experienced by the emitted electrons as a result of the bias field. This thesis will provide the relationship between the DC magnetic bias field, the electron deflection angle and the total electron deflection length; this relationship provides the possibility to adjust deflection angles and deflection lengths to suit ground-based high power RF applications. The thesis work will also show the relationship between the deflection angle and the rectangular waveguide geometry. Further still, it will provide the mathematical relationship between the secondary electron coefficient and the deflection angle.

Geng *et al.* (1999) suggests that a small magnitude DC magnetic field placed at the *z*-axis of the electric field could completely eliminate multipacting. This thesis aims to explore this statement and hopefully come up with a supporting design model.

The design is premised on the following:

i. As stated in section 1.1.3, the secondary electron yield, δ, is proportional to the square of the angle of impact, θ^2, of an electron. This suggests that smaller angles of impact result in smaller quantities of secondary electron emission (probably leading to suppression of multipactor).

ii. An electron, e, moving with a velocity $\vec{v}$ in a steady magnetic field, $\vec{B}$, experiences a magnetic force, $\overrightarrow{F_m} = -e\vec{v}\ X\ \vec{B}$, as shown in equation (2.1). This force causes the electron to deflect off its original trajectory.

The technique of DC magnetic suppression proposed will be modeled in line with the premises i and ii above. The software tools MATLAB and MS Excel Spreadsheet will be used to both verify and validate the feasibility of the model. Hopefully, this suppression model will complement currently adopted suppression techniques.

CHAPTER 3

3.0 MATERIALS AND METHODS

Satellite-borne rectangular waveguides operate in a high vacuum space environment and also under high RF power. Both these conditions favour the initiation of the multipactor breakdown, a phenomenon that limits greatly the output power of any communication satellite. Simulation results from the research work done by Geng *et al.* (1999) suggested that an external DC magnetic field of a few Gauss of amplitude placed at the *z*-axis of the electric field (in the wave propagation direction) should be very effective in disturbing electron trajectories and could completely eliminate multipacting. Several multipaction suppression techniques are available, but the DC magnetic field technique suggested by Geng *et al.*, provides an opportunity of total suppression. However, the Geng *et al.*, model is limited to the assumption that emission velocities are perpendicular to the emission surface. In reality, electrons are emitted at random angles. The model presented in this thesis is more realistic in that it considers electron emission at random angles.

This chapter begins with the details of the configuration setup for the suppression technique and the design process for modeling the equations

i. relating the angle of deflection, Φ_D, and the DC magnetic field, B, needed to effect multipactor suppression.

ii. for determining the total deflection length, D_{B_T}, at the surface of electron impact, when $0^\circ \leq \Phi_e \leq 90^\circ$.

iii. relating the emission angle, Φ_e, deflection angle, Φ_D, and impact angle, Φ_i, necessary for the implementation of the suppression technique.

Finally, the equation derived for iii. above is used to modify Vaughan's empirical formulation, equations (1.1) to (1.3), which will then be the model for the DC magnetic field suppression technique.

3.1 External DC Magnetic Field Configurations Setup in a Rectangular Waveguide

Figure 3.1 is an illustration of a typical TE_{01} mode rectangular waveguide. The figure indicates with arrows the directions of the electric field, the DC magnetic field, the emitted electron and the electromagnetic (E-M) wave propagation. In practice, when the electric field direction reverses, the direction of emitted electrons also reverses. This reversal only changes the direction of electron deflection but has no negative effect on how the DC magnetic field affects multipactor suppression. The source of the external magnetic field is positioned such that the DC magnetic field is perpendicular to the cyclic electric field but longitudinal to the direction of E-M wave propagation (Note that the DC magnetic bias method utilizes a solenoid coil wrapped around the waveguide to generate a mild DC magnetic field in the waveguide space that bends the trajectory of multipacting electrons).

Figure 3.1 forms the basic physical configuration for the modeling done in subsequent sections. While the overall configuration is retained in fig 3.4 to *Figure* 3.6, provision is made for the

emission angle, deflection angle and impact (incidence) angle to make mathematical analysis and modeling possible.

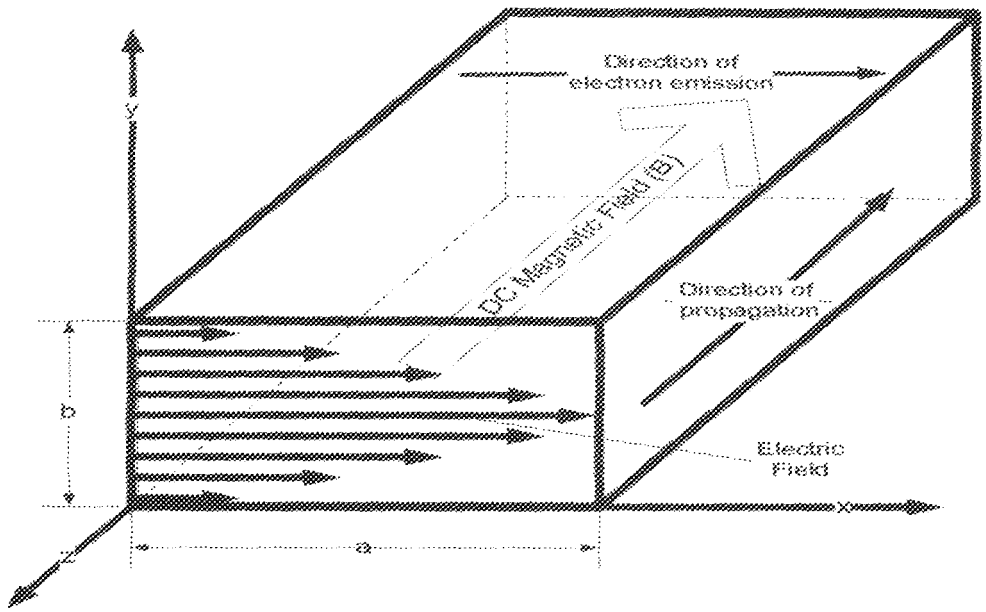

Fig. 3.1 : TE_{11} mode electric field configurations in a rectangular waveguide indicating the directions of the electric field, the emitted electron, the DC magnetic field and E-M wave propagation

3.2 Direction of Electron Motion in the Presence of a Uniform Magnetic Field

This section provides a mathematical analysis of the direction an electron emitted into a uniform magnetic field region. Because a rectangular waveguide section is the microwave component of interest for this research work, the rectangular (Cartesian) Coordinate System is employed in this analysis.

To aid the analysis, the following assumptions have been made based on the physical configuration in *Figure* 3.1.

Assumptions:

i. The uniform DC magnetic field is pointing in the z-axis direction, i.e. $\vec{B}_z$. (Note that it does not matter in which z-axis direction the magnetic field is pointing ($\vec{B}_z$ or $-\vec{B}_z$), it has the same "needed" resultant effect on the emitted electron.

ii. Electrons are emitted with different velocities at different angles.

By Lorentz force equation

$$\begin{aligned}\overrightarrow{F_m} &= q\vec{v} \times B_{a_z} \\ &= q\left(v_{a_x} + v_{a_y} + v_{a_z}\right) \times B_{a_z}\end{aligned} \tag{3.1}$$

Using vector cross multiplication

$$\begin{aligned}\overrightarrow{F_m} &= q(-vB_{a_y} + vB_{a_x}) \\ &= q(vB_{a_x} - vB_{a_y})\end{aligned} \tag{3.2}$$

This confirms that the component of $\vec{v}$ parallel to B_{a_z}, i.e v_{a_z}, does not contribute to the magnetic force. Thus, the magnitude of the magnetic force on the charged particle is expressed in terms of the components of the velocity normal to B_{a_z}.

Equation (3.2) is for a positive charge. For an electron, -e, (which is negatively charged) the equation becomes

$$\begin{aligned}\overrightarrow{F_m} &= -e(vB_{a_x} - vB_{a_y}) \\ &= e(vB_{a_y} - vB_{a_x}) \\ &= evB_{a_y} - evB_{a_x}\end{aligned} \tag{3.3}$$

which can be represented in components of $\overrightarrow{F_m}$ as,

$$\overrightarrow{F_m} = F_{m_{a_y}} - F_{m_{a_x}} \tag{3.4}$$

If the uniform magnetic field were pointing in the $-\vec{B}_z$ direction, the magnetic force influencing the direction of emitted electron motion would be in accordance with the following equations:

$$\begin{aligned} \overrightarrow{F_m} &= q\vec{v} * \left(-B_{a_z}\right) \\ &= q\left(v_{a_x} + v_{a_y} + v_{a_z}\right) * \left(-B_{a_z}\right) \end{aligned} \tag{3.5}$$

Using vector cross multiplication

$$\begin{aligned} \overrightarrow{F_m} &= q(vB_{a_y} - vB_{a_x}) \\ &= q(-vB_{a_x} + vB_{a_y}) \end{aligned} \tag{3.6}$$

Equation (3.6) is for a positive charge. For an electron, -e, the equation becomes

$$\begin{aligned} \overrightarrow{F_m} &= -e(-vB_{a_x} + vB_{a_y}) \\ &= e(vB_{a_x} - vB_{a_y}) \end{aligned} \tag{3.7}$$

which can be represented in components of $\overrightarrow{F_m}$ as,

$$\overrightarrow{F_m} = F_{m_{a_x}} - F_{m_{a_y}} \tag{3.8}$$

The significance of equations (3.4) and (3.8) is that:

I. The resultant magnetic force, $\overrightarrow{F_m}$, has components along the x-axis, $F_{m_{a_x}}$, and along the y-axis, $F_{m_{a_y}}$, but none along the z-axis.

II. The resultant magnetic force, $\overrightarrow{F_m}$, causes the moving electron to deviate off its original trajectory.

III. From equation (3.4) when the uniform magnetic field is pointing the positive z-axis direction, $\vec{B}_z$, the $F_{m_{a_y}}$ force component causes the electron to have a positive y-axis (upward) trajectory while the $F_{m_{a_x}}$ force component retards the rate of x-axis (forward) directional motion.

IV. From equation (3.8) when the uniform magnetic field is along negative z-axis, $-\vec{B}_z$, the $F_{m_{a_y}}$ force component causes the electron to have a negative y-axis (downward) trajectory while the $F_{m_{a_x}}$ force component influences a positive x-axis (forward) directional motion.

3.3 Mathematical Relationship between Deflection Angle and Uniform Magnetic Field

This section models the mathematical relationship between the deflection angle, Φ_D, and the magnetic field, B using *Figure* 3.2 and *Figure* 3.3. The deflection length is represented by D_B in *Figure* 3.2 and in Figure 3.3 and L_B is the distance over which the magnetic field is uniform (or the effective diameter of the solenoid).

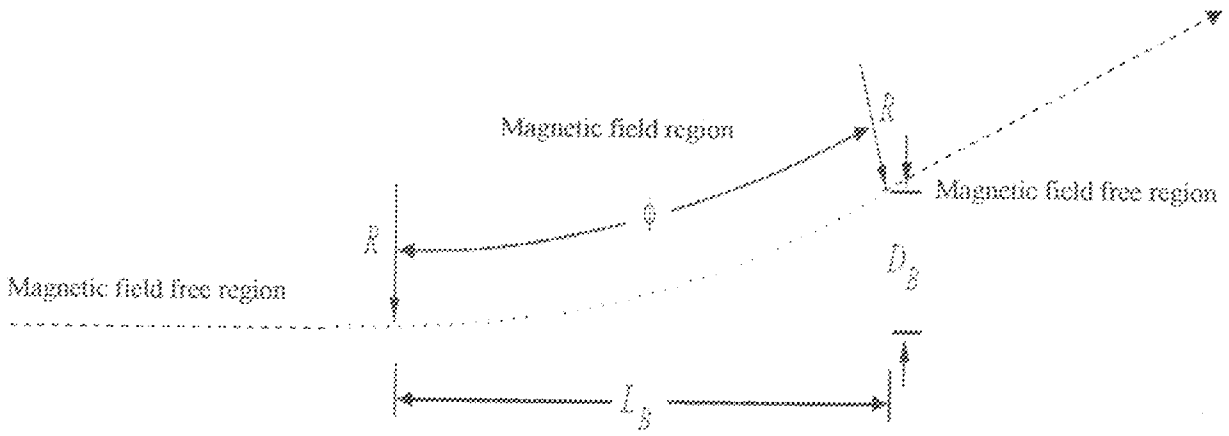

Fig.3.2 : Electron path deflection by magnetic field

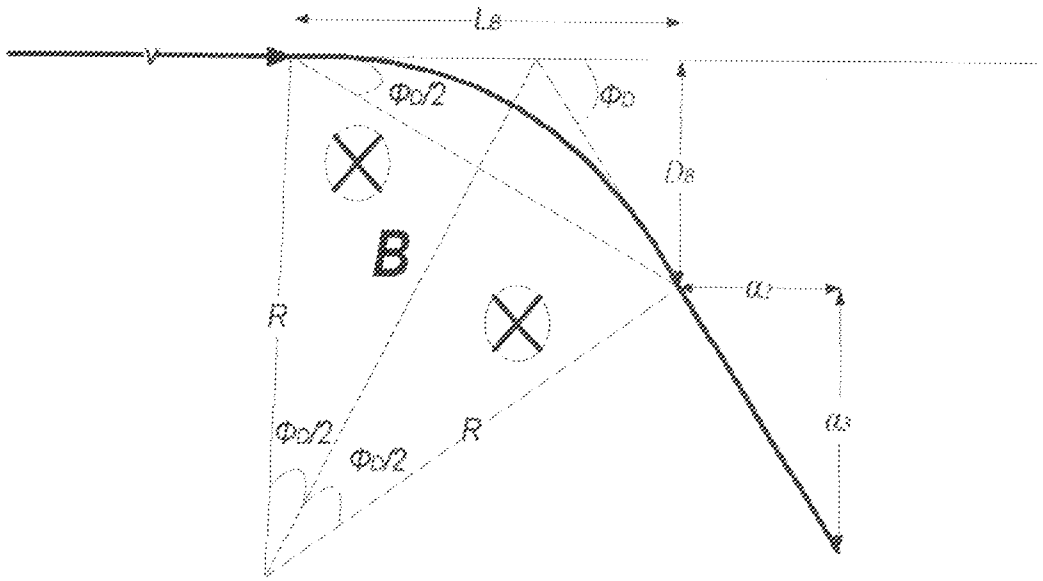

Fig 3.3 : Deflection of an electron beam by a uniform magnetic field normal to the velocity [Sears et al, 1991]

From Figure 3.3, the geometric relationship between D_B and L_B is

$$D_B = L_B \tan\left(\frac{\Phi_D}{2}\right) \tag{3.9}$$

Re-arranging equation (3.9) gives

$$\Phi_D = 2\tan^{-1}(L_B D_B) \tag{3.10}$$

Equation (3.10) provides us with the relationship between Φ_D and D_B.

For an electron with charge e, mass m_e and kinetic energy determined by an accelerating voltage V, Sears *et al.* (1991) proved that

$$D_B = \frac{eL_B^2}{\sqrt{8m_e eV}} B \tag{3.11}$$

which can also be written as

$$D_B = \frac{eL_B^2}{2m_e v} B \tag{3.12}$$

where the relationship between accelerating voltage, V, and electron velocity v is given as

$$v = \sqrt{\frac{2eV}{m_e}} \tag{3.13}$$

Equations (3.11) and (3.12) show the relationship between the deflection length, D_B, and the uniform magnetic field B.

Combining equations (3.10) and (3.11) gives the deflection angle as

$$\Phi_D = 2\tan^{-1}\left(\frac{eL_B^3}{\sqrt{8m_e eV}} B\right) \tag{3.14}$$

This is the relationship between Φ_D and B. Thus, to effect a very small deflection angle only a small uniform magnetic field is required.

Dykes *et al.* (2003) expressed the derived bias field, B, needed to fully suppress multipacting in a rectangular waveguide operated in traveling wave mode as

$$B = 4\sqrt{\frac{\mu_0 P_f}{k\omega a b^3}} \tag{3.15}$$

where P_f is the forward power, k the wave propagation constant, μ_0 the permeability of vacuum, ω the angular RF frequency, and a and b the wide and narrow dimensions of the waveguide respectively.

Combining equations (3.14) and (3.15) gives

$$\Phi_D = 2\tan^{-1}\left(\frac{2eL_B{}^3}{\sqrt{2m_e eV}}\sqrt{\frac{\mu_0 P_f}{k\omega a b^3}}\right) \tag{3.16}$$

or,

$$\Phi_D = 2\tan^{-1}\left(L_B{}^3\sqrt{\frac{2e\mu_0 P_f}{m_e V k\omega a b^3}}\right) \tag{3.17}$$

3.4 Determination of Total Deflection at $0^o \leq \Phi_e \leq 90^o$

Using Figure 3.2 and Figure 3.3, section 3.3 provided the equation for determining the length of deflection, D_B, measured from the point where the electron leaves the uniform magnetic field to the line drawn from an un-deflected electron trajectory. This section gives the total deflection length, D_{B_T}, at the surface of electron impact, working with the assumption that $0^o \leq \Phi_e \leq 90^o$.

3.4.1 Method 1: Assumption that Angles Φ_e, Φ_D and Φ_i are Known

In Figure 3.4, an electron is emitted from point A at an angle Φ_e measured from the electron trajectory to the line normal to the emission surface. It travels in a straight line until it gets to D_1 which is the point where the uniform magnetic field region begins. An electron, e, moving with a velocity v in a steady magnetic field, B, experiences a magnetic force, $F_m = -ev * B$, which can be derived from equation (2.1) or equation (3.1). The magnetic force is not only perpendicular to the magnetic field but is also normal to the direction of motion of the electron. The magnetic field does influence the direction of the motion of the electron. If the magnetic field is uniform, the force (whose direction can be determined by the right-hand rule) acting on the electron will be constant; that is the normal component of v will have a constant magnitude at any point in a plane perpendicular to the B field causing the electron to deflect, producing a circular motion. Thus, immediately the electron enters the region of uniform magnetic field, its trajectory is deflected, but only slightly, because B is very small. Deflection continues until it gets to D_2 which is the end of the magnetic field region. The electron then continues in straight trajectory until it impacts the other surface at an angle Φ_i.

Figure 3.4 shows that

$$D_{BT} = \alpha_1 + \alpha_2 + \alpha_3 \tag{3.18}$$

and

$$\alpha_3 = n * tan\,\Phi_i \tag{3.19}$$

where n is the distance between the end of the uniform magnetic field (or the end of the solenoid) and the end of the broad side of the waveguide. Also,

$$\alpha_2 = L_B * \tan\frac{\Phi_D}{2} \tag{3.20}$$

and

$$\alpha_3 = n * \tan\Phi_e \tag{3.21}$$

Summing equation (3.26), equation (3.27) and equation (3.28) gives

$$D_{BT} = n * \tan\Phi_i + L_B * \tan\frac{\Phi_D}{2} + n * \tan\Phi_e \tag{3.22}$$

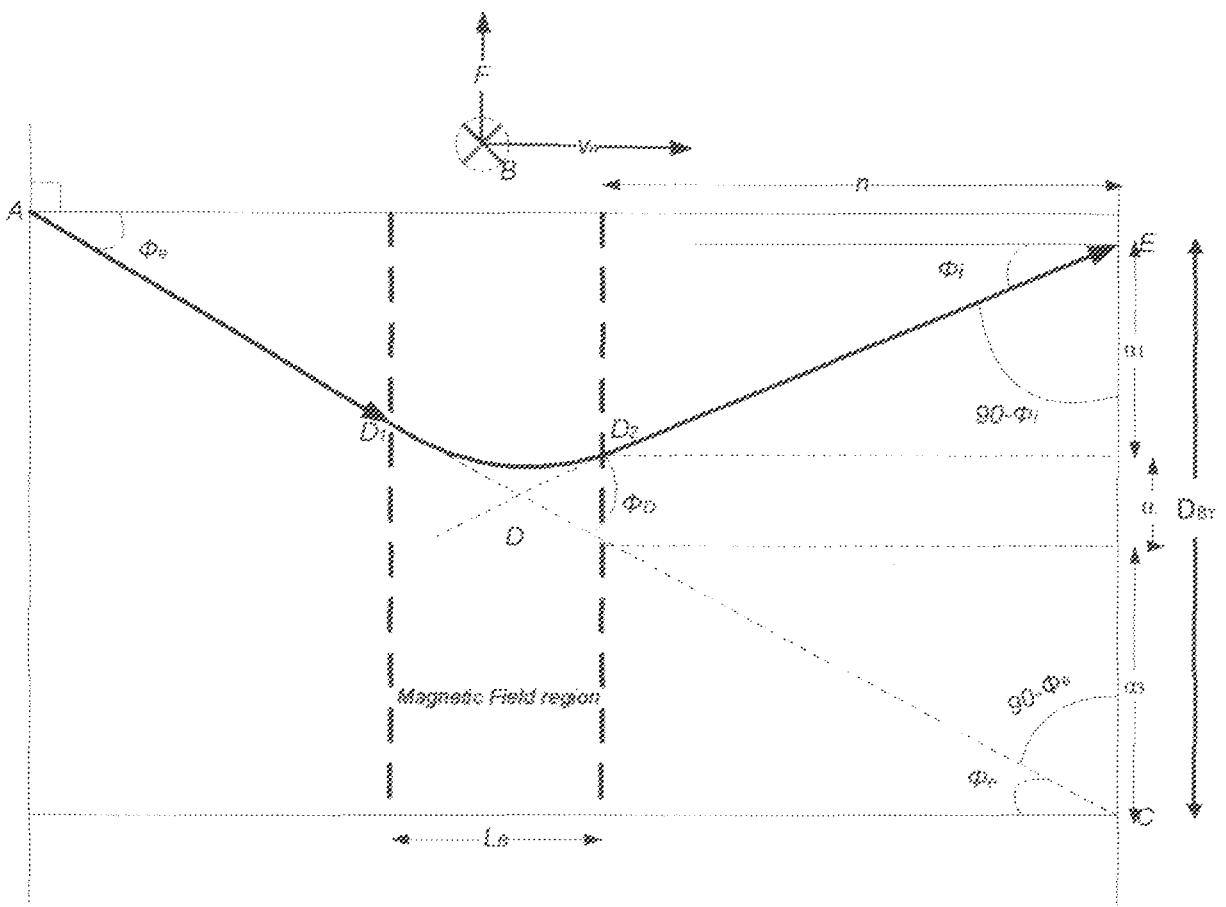

Fig. 3.4: Determination of Total Deflection when Φ_e, Φ_D and Φ_i are known at $0° \leq \Phi_e \leq 90°$

3.4.2 Method 2: Assumption that Angles Φ_e, Φ_D and Φ_I are Unknown

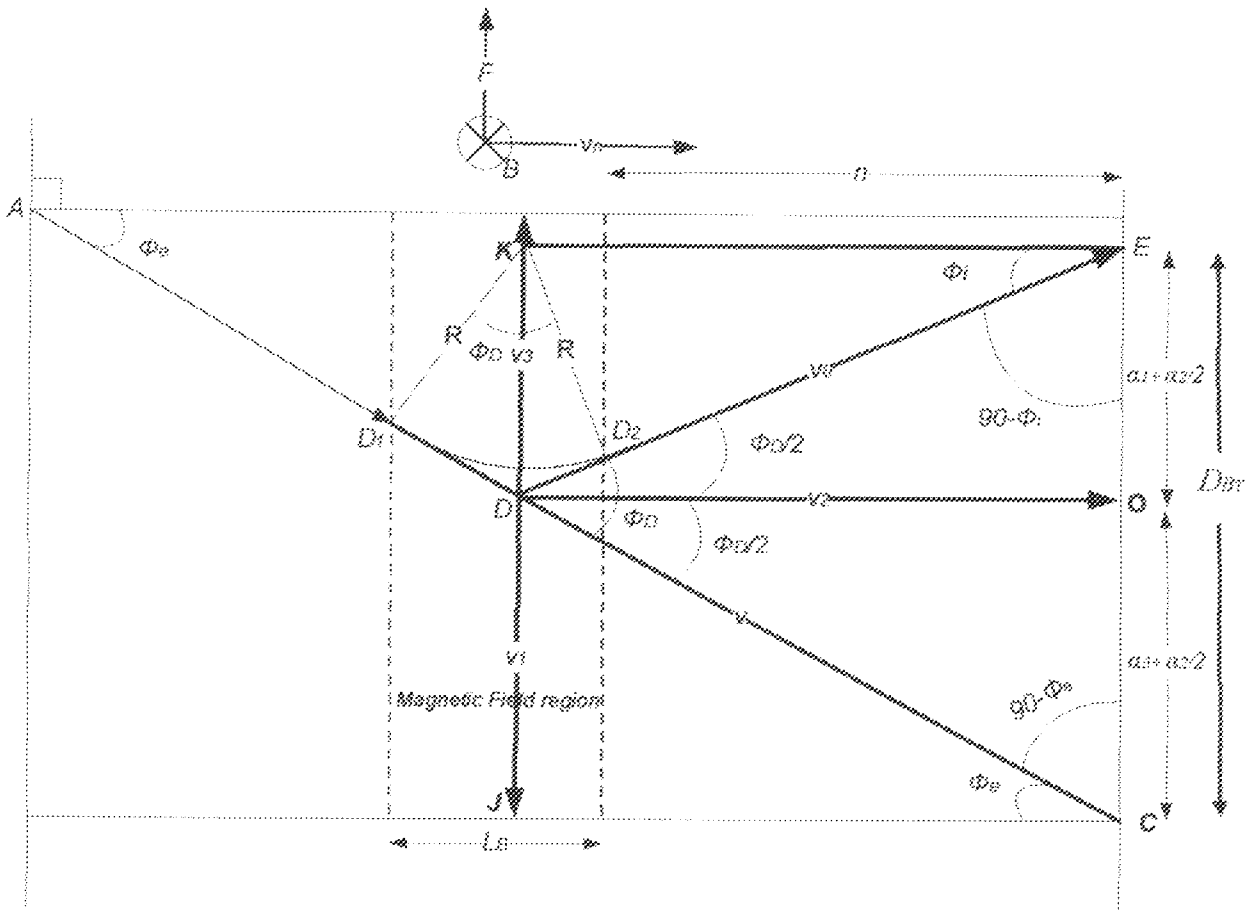

Fig. 3.5 : Determination of Total Deflection when Φ_e, Φ_D and Φ_I are unknown at $0° \leq \Phi_e \leq 90°$

From Figure 3.5,

1. An electron emitted from point *A* travels with a velocity *v* represented by the un-deflected line *AC*. This emission velocity can be used to compute for the components v_1 and v_2, as well as v_D and v_3.

2. The line representing velocity v_2 is drawn from point *D* to point *O* and it divides Φ_D and α_2 each into two equal parts.

3. The line KJ passes through point D. This line is assumed to divide L_B (the distance over which the magnetic field is uniform or the effective diameter of the solenoid) into two equal parts.

By simple geometric and trigonometric principle,

$$v_1 = v \sin\frac{\Phi_D}{2} \tag{3.23}$$

$$v_2 = v \cos\frac{\Phi_D}{2} \tag{3.24}$$

If the deflection angle is small, it can be reasonably assumed that $v = v_0$. Hence,

$$v_2 = v \sin\frac{\Phi_D}{2} \tag{3.25}$$

Using the principle of similar triangles

$$\frac{v_3}{v_2} = \frac{\alpha_1 + \frac{\alpha_2}{2}}{n + \frac{L_B}{2}} \tag{3.26}$$

where n is the distance between the end of the uniform magnetic field (or the end of the solenoid) and the end of the broad side of the waveguide.

$$\frac{v \sin\frac{\Phi_D}{2}}{v \cos\frac{\Phi_D}{2}} = \frac{\alpha_1 + \frac{\alpha_2}{2}}{n + \frac{L_B}{2}} \tag{3.27}$$

or,

$$tan\frac{\Phi_D}{2} = \frac{\alpha_1 + \frac{\alpha_2}{2}}{n + \frac{L_B}{2}} \tag{3.28}$$

Assuming that Φ_D is small and in radians, then, $\tan\frac{\Phi_D}{2} \approx \frac{\Phi_D}{2}$. Thus,

$$\frac{\Phi_D}{2} = \frac{\alpha_1 + \frac{\alpha_2}{2}}{n + \frac{L_B}{2}} \tag{3.29}$$

An electron in a magnetic field moves in a circle of radius R and is deflected through an angle Φ_D (in radians) which, according to Sears *et al.* (1991), can be expressed as

$$\Phi_D = \omega T \tag{3.30}$$

where T is the time spent in the field. Letting $n + \frac{L_B}{2} = d$, equation (3.29) becomes

$$\frac{\omega T}{2} = \frac{\alpha_1 + \frac{\alpha_2}{2}}{d} \tag{3.31}$$

Since Φ_D is assumed small in Figure 3.5,

$$T \approx \frac{L_B}{v} \tag{3.32}$$

Equation (3.31) becomes

$$\frac{\omega L_B}{2v} = \frac{\alpha_1 + \frac{\alpha_2}{2}}{d} \tag{3.33}$$

Therefore,

$$\alpha_1 + \frac{\alpha_2}{2} = \frac{\omega t L_B}{2v} \tag{3.34}$$

The speed of an electron travelling in a circle is the circumference of the circle divided by the period. That is,

$$v = \frac{2\pi R}{T} = 2\pi f R = \omega R \tag{3.35}$$

where ω is the angular velocity or angular frequency of the circular motion and can be expressed as

$$\omega = \frac{v}{R} = \frac{e}{m_e} B \tag{3.36}$$

Replacing ω from equation (3.36) and v from equation (3.13), then equation (3.34) becomes

$$\alpha_1 + \frac{\alpha_2}{2} = \frac{dL_B}{2} B \sqrt{\frac{e}{2m_e V}} \tag{3.37}$$

Following the same logical sequence

$$\alpha_3 + \frac{\alpha_2}{2} = \frac{dL_B}{2} B \sqrt{\frac{e}{2m_e V}} \tag{3.38}$$

Recall from equation (3.18) that

$$D_{BT} = \alpha_1 + \alpha_2 + \alpha_3 \tag{3.39}$$

which is the same as

$$D_{BT} = \alpha_1 + \frac{\alpha_2}{2} + \alpha_3 + \frac{\alpha_2}{2} \tag{3.40}$$

Thus, the total deflection, D_{BT}, for any emission angle such that $0^o \leq \Phi_e \leq 90^o$, can be expressed from equation (3.37), (3.38) and (3.40) as

$$D_{BT} = dL_B B \sqrt{\frac{e}{2m_e V}} \tag{3.41}$$

3.5 Modelling of the Geometric Relationship between Emission Angle, Deflection Angle and Impact Angle

This section models the equation relating the electron emission angle Φ_e, deflection angle Φ_D and impact (incidence) angle Φ_I. The following assumptions are made in this modeling exercise:

I. The length (gap) dimension of the *a*-side (broad side, between the *y*-axis parallel plates) of the rectangular waveguide is small ensuring a straight electron trajectory.

II. The electron is emitted at an angle greater than zero, measuring from the line normal to the emission surface.

III. The DC (uniform) magnetic field B is small (measured in Gauss units) resulting in a small deflection angle, most probably much less than 5°.

IV. The resultant deflection angle Φ_D is constant for all emissions since B is uniform.

V. The magnetic field is perpendicular to the RF field pointing in the positive *z*-axis (out of this paper). The electron is emitted with a velocity moving from left to right of the rectangular waveguide. Using the right-hand rule, the force acting on the electron is pointing in the positive *y*-axis (i.e. upward as opposed to downward for a positive charge).

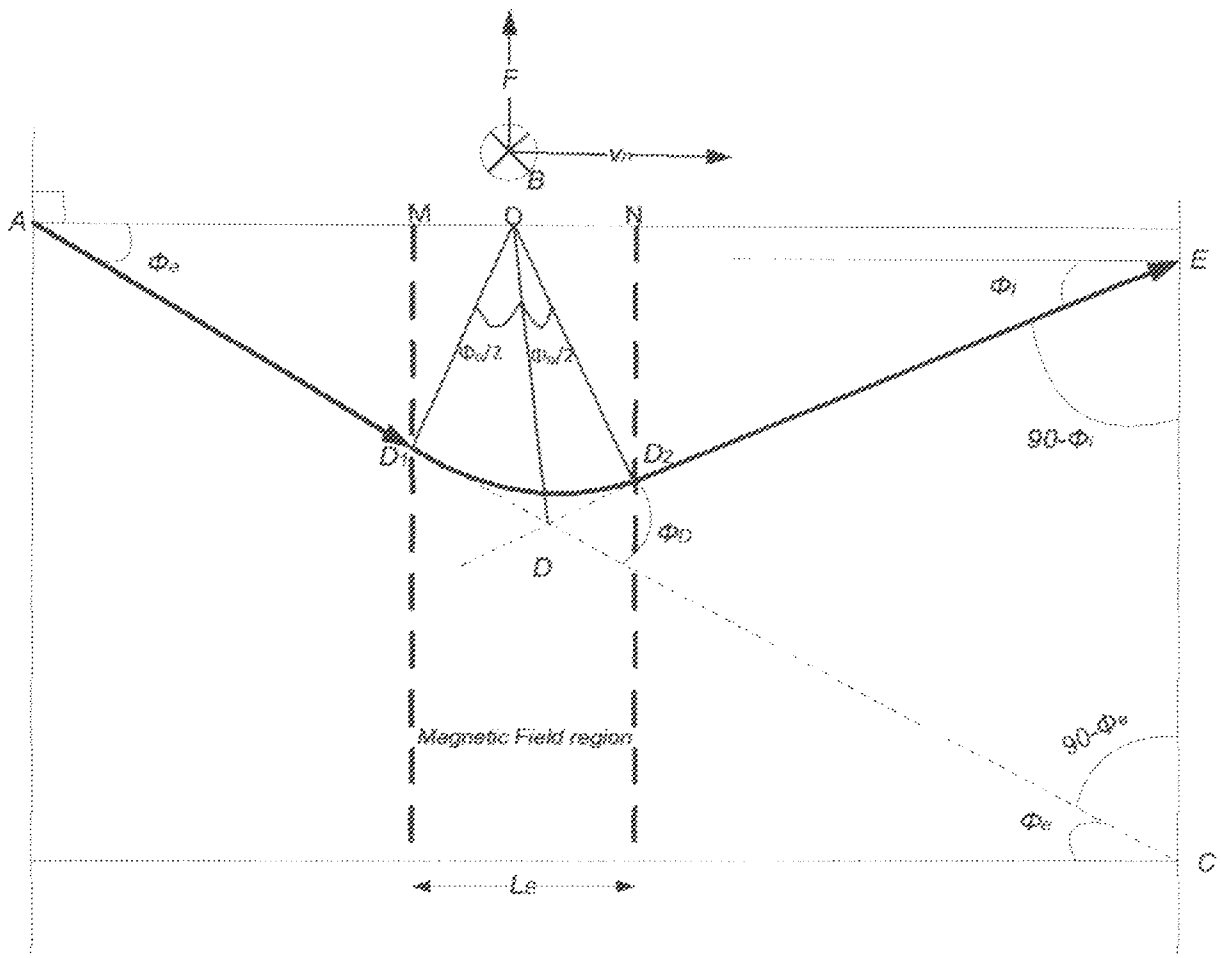

Fig. 3.6 : Modeling equation relating emission angle Φ_e, deflection angle Φ_D, and impact angle Φ_i

In Figure 3.6, an electron is emitted from point A at an angle Φ_e measured from the electron trajectory to the line normal to the emission surface. It travels in a straight line until it gets to D_1 which is the point where the uniform magnetic field region begins. Immediately the electron enters the region of the uniform magnetic field, its trajectory is deflected, but only slightly, because B is very small. Deflection continues until it gets to D_2 which is the end of the magnetic field region. The electron then continues in straight trajectory until it impacts the other surface at an angle Φ_i.

In the absence of a DC magnetic field, an electron emitted from one surface at angle Φ_e would result in impact angle Φ_i of the same magnitude at the opposite surface, giving $\Phi_i = \Phi_e$. This means that for large values of Φ_e, there is a high probability of obtaining a $SEY > 1$.

To obtain the mathematical model for the geometric relationship between emission angle Φ_e, deflection angle, Φ_D, and impact angle, Φ_i, line OD is assumed parallel to MD_1 and ND_2 because the distances D_1D and D_2D travelled by the electron during the deflection are so small that both distances can be said to be equal.

Therefore, from Figure 3.6 using the triangle DEC,

$$\Phi_D = \Phi_e + \Phi_i \tag{3.42}$$

Equation (3.42) establishes the relationship between the deflection angle, Φ_D, emission angle, Φ_e, and impact angle, Φ_i. The following deductions can be inferred from the equation:

I. The deflection angle is the sum of the emission angle and the impact angle.

II. Since Φ_D is assumed small and constant (from assumptions III and IV on page 48), if Φ_e is large, Φ_i will be negative to maintain a constant Φ_D. This negativity simply implies a change in the direction of the deflection.

Re-arranging equation (3.42) and making Φ_i the subject of the formula gives

$$\Phi_i = \Phi_D - \Phi_e \tag{3.43}$$

3.6 Modification of Vaughan's Empirical Formulation

This section uses the equation derived in the last section to modify Vaughan's empirical formulation described by equations (1.1) to (1.3) in order to provide the relationship between δ, Φ_D and Φ_e.

Combining equation (3.43) and Vaughan's empirical formulation gives equations (3.44) and (3.45).

$$E_{max}(\Phi_i) = E_{max}(0)\left(1 + \frac{k_{ss}(\Phi_D - \Phi_e)^2}{\pi}\right) \tag{3.44}$$

$$\delta_{max}(\Phi_i) = \delta_{max}(0)\left(1 + \frac{k_{ss}(\Phi_D - \Phi_e)^2}{2\pi}\right) \tag{3.45}$$

where $\delta_{max}(\Phi_i)$ is the maximum value of δ at Φ_i impact angle, $E_{max}(\Phi_i)$ is the impact energy at Φ_i impact angle which yields $\delta_{max}(\Phi_i)$, k_{ss} and k_{ss} are separate smoothness factors for the primary energy (E_p) and δ, ranging from 0 to about 2.0, with a default value of 1.0 for typical surfaces.

Equations (3.44) and (3.45) together give equation (3.46) for evaluating the δ at any given primary impact energy.

$$\delta = \delta(E_i) = \delta_{max}\left(\frac{E_i}{E_{max}} e^{1-\frac{E_i}{E_{max}}}\right)^k \tag{3.46}$$

This can be expanded to give equation (3.47) which represents the design model for DC magnetic field multipaction suppression technique.

$$\delta = \delta(E_i) = \delta_{max}(0)\left(1 + \frac{k_{s\delta}(\Phi_D - \Phi_e)^2}{2\pi}\right) *$$

$$\left(\frac{E_i}{E_{max}(0)\left(1+\frac{k_{s\varepsilon}(\Phi_D-\Phi_e)^2}{\pi}\right)} e^{\left(1-\frac{E_i}{E_{max}(0)\left(1+\frac{k_{s\varepsilon}(\Phi_D-\Phi_e)^2}{\pi}\right)}\right)}\right)^k \tag{3.47}$$

The significance of the model equations (3.43) and (3.47) with respect to multipactor suppression is that

I. Φ_i is always 'Φ_D*less than*' Φ_e for $\Phi_e > \Phi_D$. Recall from section 3.5 (and Figure 3.6), that in the absence of a DC magnetic field, an electron emitted from one surface at angle Φ_e would result in impact angle Φ_i of the same magnitude at the opposite surface, giving $\Phi_i = \Phi_e$. Meaning that for large values of Φ_e, there is a high probability of obtaining a $\delta > 1$. Thus in the presence of a DC magnetic field, for values of $\Phi_e > \Phi_D$, the angle of impact Φ_i will be less than it would have been had the uniform magnetic field been absent. This reduction in Φ_i means a reduction in the δ and hence a suppression of multipaction.

II. The relationship between $\Phi_D$and δ has been established. Since $B \propto \Phi_D$ as shown in equation (3.10), it is possible therefore to determine the value of Φ_D by varying B until a suitable δ is arrived at that will not encourage multipaction.

III. For microwave components such as rectangular waveguide that will be space borne, given any range of emission angles, it is possible to design the needed deflection angle using DC magnetic field that will result in suppression of multipaction

IV. For ground-based systems that are operated at set emission angles, Φ_e, a value for Φ_D needed for the proper working of the system can be maintained within the accepted range.

CHAPTER FOUR

4.0 RESULTS

Validation exercises and test results proving the feasibility of the suppression technique are provided in this chapter in both numerical and graphical forms. The software tools MS Excel Spreadsheet® and MATLAB® were used.

4.1 Graphical Analysis using MATLAB

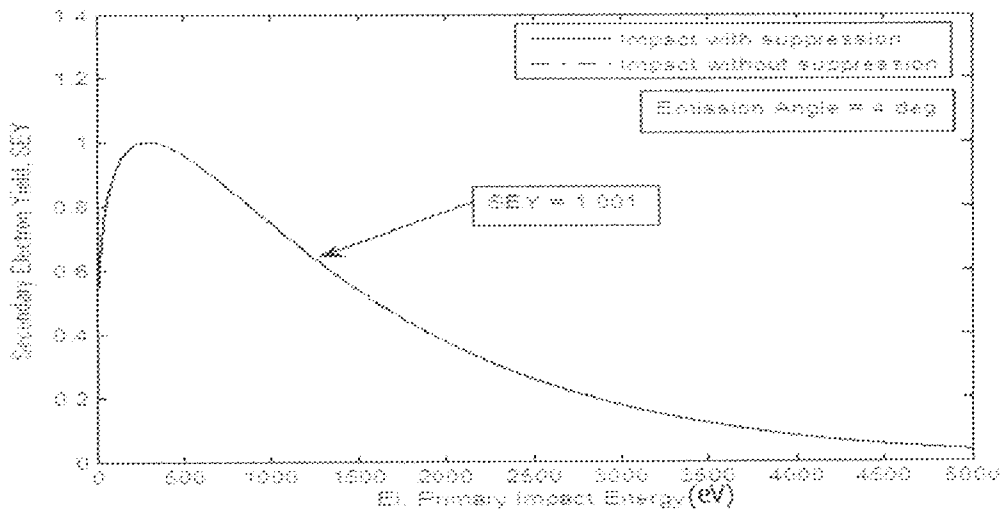

Fig. 4.1 : Plot of *SEY* to primary impact energy at 10° deflection angle and 4° emission angle

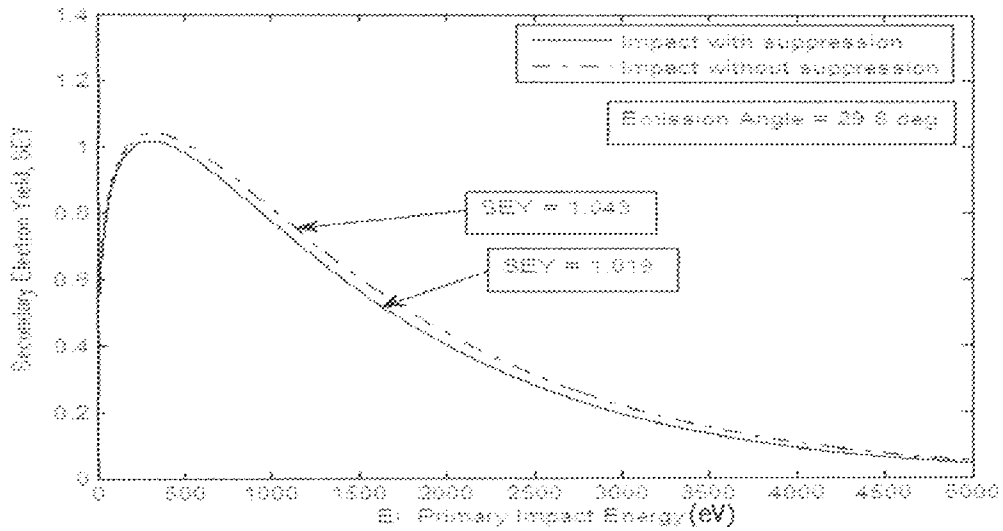

Fig. 4.2: Plot of *SEY* to primary impact energy at 10° deflection angle and 29.8° emission angle

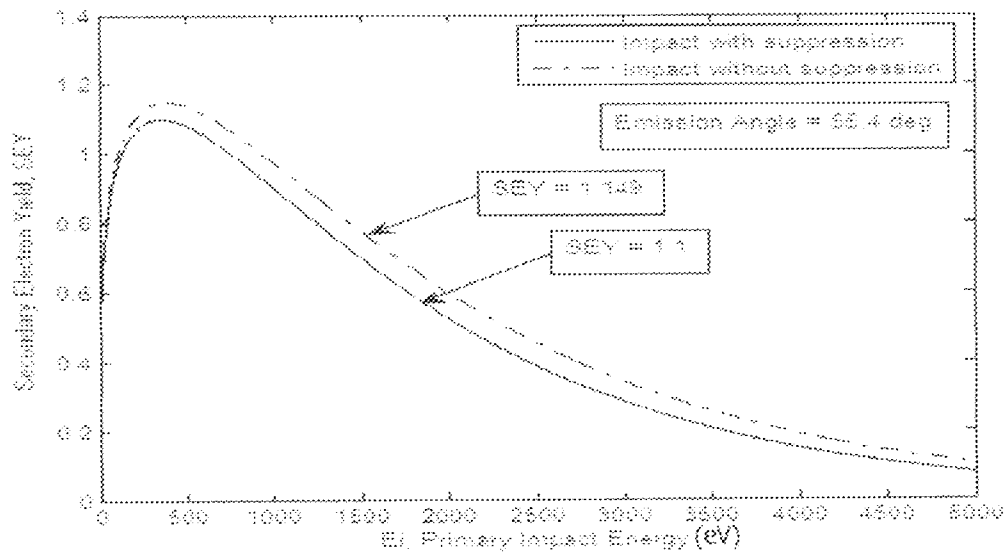

Fig. 4.3 :Plot of *SEY* to primary impact energy at 10° deflection angle and 55.4° emission angle

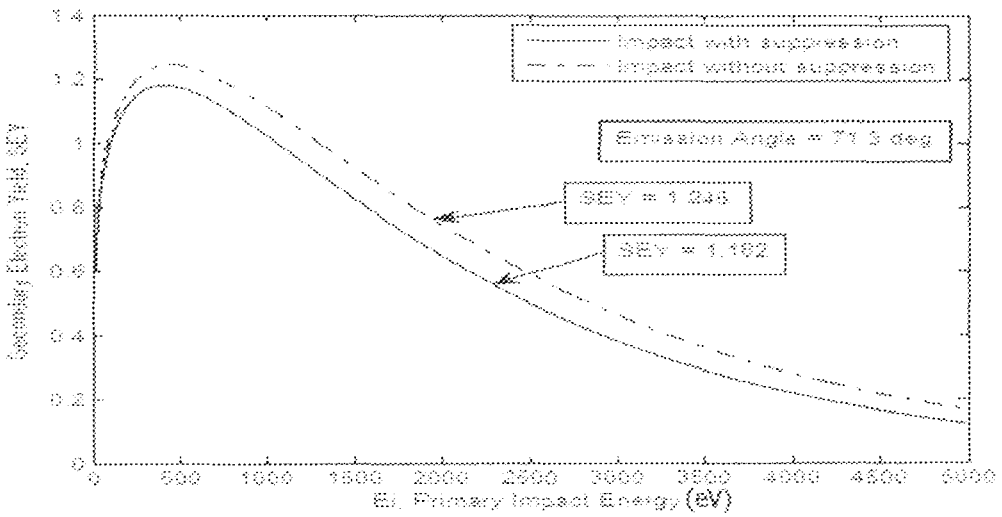

Fig. 4.4: Plot of *SEY* to primary impact energy at 10° deflection angle and 71.3° emission angle

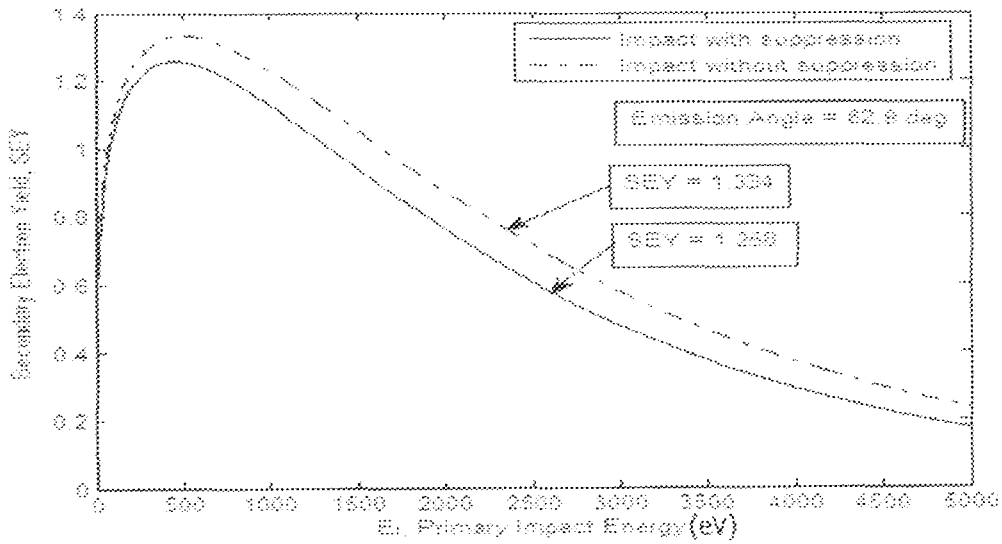

Fig. 4.5: Plot of *SEY* to primary impact energy at 10° deflection angle and 82.9° emission angle

CHAPTER FIVE

5.0 DISCUSSION, CONCLUSIONS AND RECOMMENDATIONS

5.1 Result Discussion

5.1.1 Discussion on the generated Table

Simple numerical analysis done using the analysis tool MS Excel Spreadsheet confirms the feasibility of using the DC magnetic field multipactor suppression technique.

Table 4.1 is a table that provides the numerical values of δ for corresponding deflection angles, Φ_D, and emission angles, Φ_e, at $E_{max}(0) = 300eV$ and $\delta_{max}(0) = 1$. Each value of Φ_D was inserted into equation (3.47) for each value of Φ_e to obtain δ. The values of the deflection angle are in the range $0^o \leq \Phi_D \leq 90^o$ while the emission angles are also in the range $0^o \leq \Phi_e \leq 90^o$.

In the table, the values in columns $\Phi_{D\ (deg)}$ and $\Phi_{D\ (rad)}$ represent the deflection angles in both degree and radian equivalents respectively while the values on rows $\Phi_{e(deg)}$ and $\Phi_{e(rad)}$ represent the emission angles in both degree and radian equivalents respectively. The numerical quantities in column δ are the values of δ for corresponding deflection angles, Φ_D, and emission angles, Φ_e.

Purpose of the Table

i. The table provides numerical comparison of the δ for un-deflected electron impact and that of a deflected electron impact. Values of δ when $\Phi_D = 0^o$ give the δ values for un-deflected electron impact while values of δ when $\Phi_D \neq 0^o$ gives the δ values for a deflected electron impact.

ii. It provides confirmation that the presence of a DC magnetic field really provides the possibility of multipactor suppression. This is because, generally, the values of δ at $\Phi_D > 0^\circ$ (i e. in the presence of a DC magnetic field) is lower than when $\Phi_D = 0^\circ$ (i.e. in the absence of a DC magnetic field).

How to use the Table

I. Select a deflection angle, Φ_D

II. Select an emission angle, Φe

III Locate the intersecting cell for the selected deflection and emission angles. The value in the intersecting cell is the δ for the selected deflection and emission angles.

The following shows two example cases to explain the use of the table.

Case 1: In the presence of a constant magnetic field, there is a deflection of electrons. For this scenario, $\Phi_D \neq 0^\circ$ and $\Phi_i \neq \Phi_e$.

For example:

i. Given a Φ_D of 20° and Φ_e of 17.5°, the intersecting cell has a value of 1.000303. Thus the δ is 1.000303.

ii. Given a Φ_D of 37.5° and Φ_e of 7.5°, the intersecting cell has a value of 1.04271. Thus the δ is 1.04271.

Case 2: In the absence of a constant magnetic field, there is no deflection of electrons. For this scenario, $\Phi_D = 0^\circ$ and $\Phi_i = \Phi_e$. Recall from section 3.5 (and Figure 3.6) that, in the absence of a DC magnetic field, an electron emitted from one surface at angle Φ_e would result in impact angle

Φ_i of the same magnitude at the opposite surface, giving $\Phi_i = \Phi_e$. From Vaughan's empirical formulation, $\delta \propto \Phi_i$, meaning that large values of Φ_e have a high probability of obtaining a δ>1.

Using the examples above:

i. $\Phi_D = 0^\circ$, and $\Phi_e = \Phi_i = 17.5^\circ$, thus, $\delta = 1.014736$

ii. $\Phi_D = 0^\circ$, and $\Phi_e = \Phi_i = 7.5^\circ$, thus, $\delta = 1.002723$

Table 4.1: Table of *SEY* for $0^{\circ}<\Phi_{D}\leq 90^{\circ}$ and $0^{\circ}<\Phi_{e}\leq 90^{\circ}$ at $E_{max}(0) = 300eV$ and $\delta_{max}(0) = 1$

	Φ_{Deg}	0	2.5	5	7.5	10	12.5	15	17.5	20	22.5
	Φ_{Grad}	0	0.043633	0.08727	0.1309	0.17453	0.21817	0.2618	0.30543	0.34907	0.3927
S/N	Φ_{Deg}	Φ_{Grad}	δ								
1	0.0	0.000000	1	1.000303	1.001211	1.002723	1.004836	1.007546	1.010848	1.014736	1.019203	1.024243
2	2.5	0.043633	1.000303	1	1.000303	1.001211	1.002723	1.004836	1.007546	1.010848	1.014736	1.019203
3	5.0	0.087266	1.001211	1.000303	1	1.000303	1.001211	1.002723	1.004836	1.007546	1.010848	1.014736
4	7.5	0.130900	1.002723	1.0012113	1.000303	1	1.000303	1.001211	1.002723	1.004836	1.007546	1.010848
5	10.0	0.174533	1.004836	1.0027232	1.001211	1.000303	1	1.000303	1.001211	1.002723	1.004836	1.007546
6	12.5	0.218166	1.007546	1.004836	1.002723	1.001211	1.000303	1	1.000303	1.001211	1.002723	1.004836
7	15.0	0.261799	1.010848	1.0075457	1.004836	1.002723	1.001211	1.000303	1	1.000303	1.001211	1.002723
8	17.5	0.305433	1.014736	1.0108475	1.007546	1.004836	1.002723	1.001211	1.000303	1	1.000303	1.001211
9	20.0	0.349066	1.019203	1.0147355	1.010848	1.007546	1.004836	1.002723	1.001211	1.000303	1	1.000303
10	22.5	0.392699	1.024243	1.0192031	1.014736	1.010848	1.007546	1.004836	1.002723	1.001211	1.000303	1
11	25.0	0.436332	1.029846	1.0242427	1.019203	1.014736	1.010848	1.007546	1.004836	1.002723	1.001211	1.000303
12	27.5	0.479966	1.036005	1.0298463	1.024243	1.019203	1.014736	1.010848	1.007546	1.004836	1.002723	1.001211
13	30.0	0.523599	1.04271	1.036005	1.029846	1.024243	1.019203	1.014736	1.010848	1.007546	1.004836	1.002723
14	32.5	0.567232	1.049951	1.0427099	1.036005	1.029846	1.024243	1.019203	1.014736	1.010848	1.007546	1.004836
15	35.0	0.610865	1.057719	1.0499512	1.04271	1.036005	1.029846	1.024243	1.019203	1.014736	1.010848	1.007546
16	37.5	0.654498	1.066004	1.0577192	1.049951	1.04271	1.036005	1.029846	1.024243	1.019203	1.014736	1.010848
17	40.0	0.698132	1.074795	1.0660039	1.057719	1.049951	1.04271	1.036005	1.029846	1.024243	1.019203	1.014736
18	42.5	0.741765	1.084083	1.0747952	1.066004	1.057719	1.049951	1.04271	1.036005	1.029846	1.024243	1.019203
19	45.0	0.785398	1.093857	1.084083	1.074795	1.066004	1.057719	1.049951	1.04271	1.036005	1.029846	1.024243
20	47.5	0.829031	1.104108	1.0938573	1.084083	1.074795	1.066004	1.057719	1.049951	1.04271	1.036005	1.029846
21	50.0	0.872665	1.114826	1.1041082	1.093857	1.084083	1.074795	1.066004	1.057719	1.049951	1.04271	1.036005
22	52.5	0.916298	1.126001	1.1148259	1.104108	1.093857	1.084083	1.074795	1.066004	1.057719	1.049951	1.04271
23	55.0	0.959931	1.137624	1.126001	1.114826	1.104108	1.093857	1.084083	1.074795	1.066004	1.057719	1.049951
24	57.5	1.003564	1.149687	1.1376242	1.126001	1.114826	1.104108	1.093857	1.084083	1.074795	1.066004	1.057719

	$\Phi_{2(deg)}$	0	2.5	5	7.5	10	12.5	15	17.5	20	22.5
	$\Phi_{2(rad)}$	0	0.043633	0.08727	0.1309	0.17453	0.21817	0.2618	0.30543	0.34907	0.3927
S/N	$\Phi_{1(deg)}$	$\Phi_{1(rad)}$	δ								
25	60.0	1.047198	1.16218	1.1496867	1.137624	1.126001	1.114826	1.104108	1.093857	1.084083	1.074795	1.066004
26	62.5	1.090831	1.175095	1.1621798	1.149687	1.137624	1.126001	1.114826	1.104108	1.093857	1.084083	1.074795
27	65.0	1.134464	1.188425	1.1750952	1.16218	1.149687	1.137624	1.126001	1.114826	1.104108	1.093857	1.084083
28	67.5	1.178097	1.202162	1.1884251	1.175095	1.16218	1.149687	1.137624	1.126001	1.114826	1.104108	1.093857
29	70.0	1.221730	1.216298	1.2021617	1.188425	1.175095	1.16218	1.149687	1.137624	1.126001	1.114826	1.104108
30	72.5	1.265364	1.230827	1.2162979	1.202162	1.188425	1.175095	1.16218	1.149687	1.137624	1.126001	1.114826
31	75.0	1.308997	1.245742	1.2308267	1.216298	1.202162	1.188425	1.175095	1.16218	1.149687	1.137624	1.126001
32	77.5	1.352630	1.261036	1.2457416	1.230827	1.216298	1.202162	1.188425	1.175095	1.16218	1.149687	1.137624
33	80.0	1.396263	1.276705	1.2610362	1.245742	1.230827	1.216298	1.202162	1.188425	1.175095	1.16218	1.149687
34	82.5	1.439897	1.292741	1.2767047	1.261036	1.245742	1.230827	1.216298	1.202162	1.188425	1.175095	1.16218
35	85.0	1.483530	1.309141	1.2927413	1.276705	1.261036	1.245742	1.230827	1.216298	1.202162	1.188425	1.175095
36	87.5	1.527163	1.325897	1.3091406	1.292741	1.276705	1.261036	1.245742	1.230827	1.216298	1.202162	1.188425
37	90.0	1.570796	1.343007	1.3258975	1.309141	1.292741	1.276705	1.261036	1.245742	1.230827	1.216298	1.202162

	$\Phi_{2(deg)}$	25	27.5	30	32.5	35	37.5	40	42.5	45	47.5
	$\Phi_{2(rad)}$	0.43633	0.47997	0.5236	0.56723	0.61087	0.6545	0.69813	0.74176	0.7854	0.82903
S/N	$\Phi_{1(deg)}$	$\Phi_{1(rad)}$	δ								
1	0.0	0.000000	1.029846	1.036005	1.04271	1.049951	1.057719	1.066004	1.074795	1.084083	1.093857	1.104108
2	2.5	0.043633	1.024243	1.029846	1.036005	1.04271	1.049951	1.057719	1.066004	1.074795	1.084083	1.093857
3	5.0	0.087266	1.019203	1.024243	1.029846	1.036005	1.04271	1.049951	1.057719	1.066004	1.074795	1.084083
4	7.5	0.130900	1.014736	1.019203	1.024243	1.029846	1.036005	1.04271	1.049951	1.057719	1.066004	1.074795

	$\Phi_{prilagi}$		25	27.5	30	32.5	35	37.5	40	42.5	45	47.5
	$\Phi_{prilagi}$		0.43633	0.47997	0.5236	0.56723	0.61087	0.6545	0.69813	0.74176	0.7854	0.82903
S/N	$\Phi_{Prilagi}$	$\Phi_{Prirodi}$	δ									
5	10.0	0.174533	1.010848	1.014736	1.019203	1.024243	1.029846	1.036005	1.04271	1.049951	1.057719	1.066004
6	12.5	0.218166	1.007546	1.010848	1.014736	1.019203	1.024243	1.029846	1.036005	1.04271	1.049951	1.057719
7	15.0	0.261799	1.004836	1.007546	1.010848	1.014736	1.019203	1.024243	1.029846	1.036005	1.04271	1.049951
8	17.5	0.305433	1.002723	1.004836	1.007546	1.010848	1.014736	1.019203	1.024243	1.029846	1.036005	1.04271
9	20.0	0.349066	1.001211	1.002723	1.004836	1.007546	1.010848	1.014736	1.019203	1.024243	1.029846	1.036005
10	22.5	0.392699	1.000303	1.001211	1.002723	1.004836	1.007546	1.010848	1.014736	1.019203	1.024243	1.029846
11	25.0	0.436332	1	1.000303	1.001211	1.002723	1.004836	1.007546	1.010848	1.014736	1.019203	1.024243
12	27.5	0.479966	1.000303	1	1.000303	1.001211	1.002723	1.004836	1.007546	1.010848	1.014736	1.019203
13	30.0	0.523599	1.001211	1.000303	1	1.000303	1.001211	1.002723	1.004836	1.007546	1.010848	1.014736
14	32.5	0.567232	1.002723	1.001211	1.000303	1	1.000303	1.001211	1.002723	1.004836	1.007546	1.010848
15	35.0	0.610865	1.004836	1.002723	1.001211	1.000303	1	1.000303	1.001211	1.002723	1.004836	1.007546
16	37.5	0.654498	1.007546	1.004836	1.002723	1.001211	1.000303	1	1.000303	1.001211	1.002723	1.004836
17	40.0	0.698132	1.010848	1.007546	1.004836	1.002723	1.001211	1.000303	1	1.000303	1.001211	1.002723
18	42.5	0.741765	1.014736	1.010848	1.007546	1.004836	1.002723	1.001211	1.000303	1	1.000303	1.001211
19	45.0	0.785398	1.019203	1.014736	1.010848	1.007546	1.004836	1.002723	1.001211	1.000303	1	1.000303
20	47.5	0.829031	1.024243	1.019203	1.014736	1.010848	1.007546	1.004836	1.002723	1.001211	1.000303	1
21	50.0	0.872665	1.029846	1.024243	1.019203	1.014736	1.010848	1.007546	1.004836	1.002723	1.001211	1.000303
22	52.5	0.916298	1.036005	1.029846	1.024243	1.019203	1.014736	1.010848	1.007546	1.004836	1.002723	1.001211
23	55.0	0.959931	1.04271	1.036005	1.029846	1.024243	1.019203	1.014736	1.010848	1.007546	1.004836	1.002723
24	57.5	1.003564	1.049951	1.04271	1.036005	1.029846	1.024243	1.019203	1.014736	1.010848	1.007546	1.004836
25	60.0	1.047198	1.057719	1.049951	1.04271	1.036005	1.029846	1.024243	1.019203	1.014736	1.010848	1.007546
26	62.5	1.090831	1.066004	1.057719	1.049951	1.04271	1.036005	1.029846	1.024243	1.019203	1.014736	1.010848
27	65.0	1.134464	1.074795	1.066004	1.057719	1.049951	1.04271	1.036005	1.029846	1.024243	1.019203	1.014736
28	67.5	1.178097	1.084083	1.074795	1.066004	1.057719	1.049951	1.04271	1.036005	1.029846	1.024243	1.019203
29	70.0	1.221730	1.093857	1.084083	1.074795	1.066004	1.057719	1.049951	1.04271	1.036005	1.029846	1.024243
30	72.5	1.265364	1.104108	1.093857	1.084083	1.074795	1.066004	1.057719	1.049951	1.04271	1.036005	1.029846

	Φ_{stdeg}	25	27.5	30	32.5	35	37.5	40	42.5	45	47.5
	Φ_{strad}	0.43633	0.47997	0.5236	0.56723	0.61087	0.6545	0.69813	0.74176	0.7854	0.82903
S/N	Φ_{Ldeg}	Φ_{Lrad}	δ								
31	75.0	1.308997	1.114826	1.104108	1.093857	1.084083	1.074795	1.066004	1.057719	1.049951	1.04271	1.036005
32	77.5	1.352630	1.126001	1.114826	1.104108	1.093857	1.084083	1.074795	1.066004	1.057719	1.049951	1.04271
33	80.0	1.396263	1.137624	1.126001	1.114826	1.104108	1.093857	1.084083	1.074795	1.066004	1.057719	1.049951
34	82.5	1.439897	1.149687	1.137624	1.126001	1.114826	1.104108	1.093857	1.084083	1.074795	1.066004	1.057719
35	85.0	1.483530	1.16218	1.149687	1.137624	1.126001	1.114826	1.104108	1.093857	1.084083	1.074795	1.066004
36	87.5	1.527163	1.175095	1.16218	1.149687	1.137624	1.126001	1.114826	1.104108	1.093857	1.084083	1.074795
37	90.0	1.570796	1.188425	1.175095	1.16218	1.149687	1.137624	1.126001	1.114826	1.104108	1.093857	1.084083

	Φ_{stdeg}	50	52.5	55	57.5	60	62.5	65	67.5	70	72.5
	Φ_{strad}	0.87266	0.9163	0.95993	1.00356	1.0472	1.09083	1.13446	1.1781	1.22173	1.26536
S/N	Φ_{Ldeg}	Φ_{Lrad}	δ								
1	0.0	0.000000	1.114826	1.126001	1.137624	1.149687	1.16218	1.175095	1.188425	1.202162	1.216298	1.230827
2	2.5	0.043633	1.104108	1.114826	1.126001	1.137624	1.149687	1.16218	1.175095	1.188425	1.202162	1.216298
3	5.0	0.087266	1.093857	1.104108	1.114826	1.126001	1.137624	1.149687	1.16218	1.175095	1.188425	1.202162
4	7.5	0.130900	1.084083	1.093857	1.104108	1.114826	1.126001	1.137624	1.149687	1.16218	1.175095	1.188425
5	10.0	0.174533	1.074795	1.084083	1.093857	1.104108	1.114826	1.126001	1.137624	1.149687	1.16218	1.175095
6	12.5	0.218166	1.066004	1.074795	1.084083	1.093857	1.104108	1.114826	1.126001	1.137624	1.149687	1.16218
7	15.0	0.261799	1.057719	1.066004	1.074795	1.084083	1.093857	1.104108	1.114826	1.126001	1.137624	1.149687
8	17.5	0.305433	1.049951	1.057719	1.066004	1.074795	1.084083	1.093857	1.104108	1.114826	1.126001	1.137624
9	20.0	0.349066	1.04271	1.049951	1.057719	1.066004	1.074795	1.084083	1.093857	1.104108	1.114826	1.126001
10	22.5	0.392699	1.036005	1.04271	1.049951	1.057719	1.066004	1.074795	1.084083	1.093857	1.104108	1.114826
11	25.0	0.436332	1.029846	1.036005	1.04271	1.049951	1.057719	1.066004	1.074795	1.084083	1.093857	1.104108
12	27.5	0.479966	1.024243	1.029846	1.036005	1.04271	1.049951	1.057719	1.066004	1.074795	1.084083	1.093857

	Φ_{deg}	50	52.5	55	57.5	60	62.5	65	67.5	70	72.5
	Φ_{rad}	0.87266	0.9163	0.95993	1.00356	1.0472	1.09083	1.13446	1.1781	1.22173	1.26536
S/N	Φ_{Deg}	Φ_{Rad}	δ								
13	30.0	0.523599	1.019203	1.024243	1.029846	1.036005	1.04271	1.049951	1.057719	1.066004	1.074795	1.084083
14	32.5	0.567232	1.014736	1.019203	1.024243	1.029846	1.036005	1.04271	1.049951	1.057719	1.066004	1.074795
15	35.0	0.610865	1.010848	1.014736	1.019203	1.024243	1.029846	1.036005	1.04271	1.049951	1.057719	1.066004
16	37.5	0.654498	1.007546	1.010848	1.014736	1.019203	1.024243	1.029846	1.036005	1.04271	1.049951	1.057719
17	40.0	0.698132	1.004836	1.007546	1.010848	1.014736	1.019203	1.024243	1.029846	1.036005	1.04271	1.049951
18	42.5	0.741765	1.002723	1.004836	1.007546	1.010848	1.014736	1.019203	1.024243	1.029846	1.036005	1.04271
19	45.0	0.785398	1.001211	1.002723	1.004836	1.007546	1.010848	1.014736	1.019203	1.024243	1.029846	1.036005
20	47.5	0.829031	1.000303	1.001211	1.002723	1.004836	1.007546	1.010848	1.014736	1.019203	1.024243	1.029846
21	50.0	0.872665	1	1.000303	1.001211	1.002723	1.004836	1.007546	1.010848	1.014736	1.019203	1.024243
22	52.5	0.916298	1.000303	1	1.000303	1.001211	1.002723	1.004836	1.007546	1.010848	1.014736	1.019203
23	55.0	0.959931	1.001211	1.000303	1	1.000303	1.001211	1.002723	1.004836	1.007546	1.010848	1.014736
24	57.5	1.003564	1.002723	1.001211	1.000303	1	1.000303	1.001211	1.002723	1.004836	1.007546	1.010848
25	60.0	1.047198	1.004836	1.002723	1.001211	1.000303	1	1.000303	1.001211	1.002723	1.004836	1.007546
26	62.5	1.090831	1.007546	1.004836	1.002723	1.001211	1.000303	1	1.000303	1.001211	1.002723	1.004836
27	65.0	1.134464	1.010848	1.007546	1.004836	1.002723	1.001211	1.000303	1	1.000303	1.001211	1.002723
28	67.5	1.178097	1.014736	1.010848	1.007546	1.004836	1.002723	1.001211	1.000303	1	1.000303	1.001211
29	70.0	1.221730	1.019203	1.014736	1.010848	1.007546	1.004836	1.002723	1.001211	1.000303	1	1.000303
30	72.5	1.265364	1.024243	1.019203	1.014736	1.010848	1.007546	1.004836	1.002723	1.001211	1.000303	1
31	75.0	1.308997	1.029846	1.024243	1.019203	1.014736	1.010848	1.007546	1.004836	1.002723	1.001211	1.000303
32	77.5	1.352630	1.036005	1.029846	1.024243	1.019203	1.014736	1.010848	1.007546	1.004836	1.002723	1.001211
33	80.0	1.396263	1.04271	1.036005	1.029846	1.024243	1.019203	1.014736	1.010848	1.007546	1.004836	1.002723
34	82.5	1.439897	1.049951	1.04271	1.036005	1.029846	1.024243	1.019203	1.014736	1.010848	1.007546	1.004836
35	85.0	1.483530	1.057719	1.049951	1.04271	1.036005	1.029846	1.024243	1.019203	1.014736	1.010848	1.007546
36	87.5	1.527163	1.066004	1.057719	1.049951	1.04271	1.036005	1.029846	1.024243	1.019203	1.014736	1.010848
37	90.0	1.570796	1.074795	1.066004	1.057719	1.049951	1.04271	1.036005	1.029846	1.024243	1.019203	1.014736

	Φ_{edge}	75	77.5	80	82.5	85	87.5	90
	Φ_{circle}	1.309	1.35263	1.39626	1.4399	1.48353	1.52716	1.5708
S/N	Φ_{radius}	Φ_{Dradii}			δ			
1	0.0	0.000000	1.245742	1.261036	1.276705	1.292741	1.309141	1.325897	1.343007
2	2.5	0.043633	1.230827	1.245742	1.261036	1.276705	1.292741	1.309141	1.325897
3	5.0	0.087266	1.216298	1.230827	1.245742	1.261036	1.276705	1.292741	1.309141
4	7.5	0.130900	1.202162	1.216298	1.230827	1.245742	1.261036	1.276705	1.292741
5	10.0	0.174533	1.188425	1.202162	1.216298	1.230827	1.245742	1.261036	1.276705
6	12.5	0.218166	1.175095	1.188425	1.202162	1.216298	1.230827	1.245742	1.261036
7	15.0	0.261799	1.16218	1.175095	1.188425	1.202162	1.216298	1.230827	1.245742
8	17.5	0.305433	1.149687	1.16218	1.175095	1.188425	1.202162	1.216298	1.230827
9	20.0	0.349066	1.137624	1.149687	1.16218	1.175095	1.188425	1.202162	1.216298
10	22.5	0.392699	1.126001	1.137624	1.149687	1.16218	1.175095	1.188425	1.202162
11	25.0	0.436332	1.114826	1.126001	1.137624	1.149687	1.16218	1.175095	1.188425
12	27.5	0.479966	1.104108	1.114826	1.126001	1.137624	1.149687	1.16218	1.175095
13	30.0	0.523599	1.093857	1.104108	1.114826	1.126001	1.137624	1.149687	1.16218
14	32.5	0.567232	1.084083	1.093857	1.104108	1.114826	1.126001	1.137624	1.149687
15	35.0	0.610865	1.074795	1.084083	1.093857	1.104108	1.114826	1.126001	1.137624
16	37.5	0.654498	1.066004	1.074795	1.084083	1.093857	1.104108	1.114826	1.126001
17	40.0	0.698132	1.057719	1.066004	1.074795	1.084083	1.093857	1.104108	1.114826
18	42.5	0.741765	1.049951	1.057719	1.066004	1.074795	1.084083	1.093857	1.104108
19	45.0	0.785398	1.04271	1.049951	1.057719	1.066004	1.074795	1.084083	1.093857
20	47.5	0.829031	1.036005	1.04271	1.049951	1.057719	1.066004	1.074795	1.084083
21	50.0	0.872665	1.029846	1.036005	1.04271	1.049951	1.057719	1.066004	1.074795
22	52.5	0.916298	1.024243	1.029846	1.036005	1.04271	1.049951	1.057719	1.066004
23	55.0	0.959931	1.019203	1.024243	1.029846	1.036005	1.04271	1.049951	1.057719
24	57.5	1.003564	1.014736	1.019203	1.024243	1.029846	1.036005	1.04271	1.049951

	$\Phi_{a(deg)}$	75	77.5	80	82.5	85	87.5	90
	$\Phi_{a(rad)}$	1.309	1.35263	1.39626	1.4399	1.48353	1.52716	1.5708
S/N	$\Phi_{b(deg)}$	$\Phi_{b(rad)}$				δ			
25	60.0	1.047198	1.010848	1.014736	1.019203	1.024243	1.029846	1.036005	1.04271
26	62.5	1.090831	1.007546	1.010848	1.014736	1.019203	1.024243	1.029846	1.036005
27	65.0	1.134464	1.004836	1.007546	1.010848	1.014736	1.019203	1.024243	1.029846
28	67.5	1.178097	1.002723	1.004836	1.007546	1.010848	1.014736	1.019203	1.024243
29	70.0	1.221730	1.001211	1.002723	1.004836	1.007546	1.010848	1.014736	1.019203
30	72.5	1.265364	1.000303	1.001211	1.002723	1.004836	1.007546	1.010848	1.014736
31	75.0	1.308997	1	1.000303	1.001211	1.002723	1.004836	1.007546	1.010848
32	77.5	1.352630	1.000303	1	1.000303	1.001211	1.002723	1.004836	1.007546
33	80.0	1.396263	1.001211	1.000303	1	1.000303	1.001211	1.002723	1.004836
34	82.5	1.439897	1.002723	1.001211	1.000303	1	1.000303	1.001211	1.002723
35	85.0	1.483530	1.004836	1.002723	1.001211	1.000303	1	1.000303	1.001211
36	87.5	1.527163	1.007546	1.004836	1.002723	1.001211	1.000303	1	1.000303
37	90.0	1.570796	1.010848	1.007546	1.004836	1.002723	1.001211	1.000303	1

Critical analysis of the table 4.1 shows that:

I. Generally, a deflected electron impact resulting from the presence of a DC magnetic field has a lower δ than an un-deflected electron impact.

II. The presence of a DC magnetic field reduces the δ only when the $\Phi_e \geq \frac{1}{2}\Phi_D$.

III. The deflection angles $0^\circ < \Phi_D \leq 10^\circ$ provide δ reduction for a larger range of Φ_e while $\Phi_D > 10^\circ$ provides δ reduction for a lesser range of Φ_e. This implies that it is preferable to use small deflection angles in the range $0^\circ < \Phi_D \leq 10^\circ$ to effect δ reduction hence suppressing multipaction. It has been shown in chapter three, that a small deflection angle can be effected by a small magnetic field.

5.1.2 Discussion on the generated Graphs

Figs. 4.1 to 4.5 indicate that:

i. The deflection of electrons resulting from the inclusion of a DC magnetic field does reduce the δ and may ultimately lead to reduction in multipaction. However, for emission angles less than 5° (i.e. $\Phi_e < 5^\circ$), the reduction in δ is not significant enough to be considered a suppression of multipaction, as seen in fig 4.1. This therefore suggests that the suppression technique is only useful for $\Phi_e \geq 5^\circ$.

ii. For the deflection angle considered (i.e. 10°, though this applies to the range $1^\circ \leq \Phi_D \leq 10^\circ$) the percentage suppression increases with increasing emission angle. This is shown in Table 5.1.

Table 5.1 Percentage suppression at 10^{o} deflection angle for increasing emission angle.

Emission Angle (degree)	SEY		Percentage Suppression (%)
	No Suppression	Suppression	
4.0	1.001	1.001	0.000
29.8	1.043	1.019	2.301
55.4	1.149	1.100	4.265
71.3	1.246	1.182	5.136
82.9	1.334	1.258	5.697

5.2 Conclusion

The results of this work leads to several important conclusions on the suppressive effect of a DC magnetic field on multipaction in a rectangular waveguide. It also gives the range for both the deflection angles and emission angles that provide for this suppression.

Findings

By applying a DC magnetic field, electron trajectory can be disturbed. Models and simulations have shown that an external DC magnetic field applied in the direction of wave propagation in a rectangular waveguide can efficiently suppress multipactor. The findings in this work can be reasonably summarized as follows:

I. Generally, the impact of a deflected electron (resulting from the presence of a DC magnetic field) has a lower δ than the impact of an un-deflected electron resulting in multipactor suppression.

II. The presence of a DC magnetic field reduces the δ only when the $\Phi_e \geq \frac{1}{2}\Phi_D$.

III. The deflection angles $0° < \Phi_D \leq 10°$ provide δ reduction for a larger range of Φ_e while $\Phi_D > 10°$ provide δ reduction for a lesser range of Φ_e.

IV. The deflection of electrons resulting from the inclusion of a DC magnetic field does reduce the δ and may ultimately lead to reduction in multipaction. However, the suppression technique is only useful for $\Phi_e \geq 5°$.

V. For the deflection angle considered, that is $1° \leq \Phi_D \leq 10°$, the percentage suppression increases with increasing emission angle.

5.3 Recommendations

The objective of this work was to suggest a complementary multipactor suppression technique different from the conventional surface treatment/coating and geometrical modification techniques currently used in satellite rectangular waveguides. However, the results of the research have been wholly based on derived mathematical models. The absence of advanced experimentation laboratories makes physical verification of these models impossible. Before the results of this work can be safely implemented in rectangular waveguides, a proper experimental verification process is required.

Future work on this subject should concentrate on creating better designed and more robust simulations with capabilities for tracking more accurately the trajectories and deflection angles of electrons for the rectangular waveguide geometry in the presence of magnetic fields of different strengths.

A drawback with the proposed technique is the extra components (such as solenoid) required to produce the DC magnetic field. Therefore, to make the method feasible for space applications where extra weight is undesirable, the design and manufacturing processes for the additional components should take into serious consideration the use of light-weight materials in the components development.

REFERENCES

Baglin V., Bojko I. J., Gröbner O., Henrist B., Hilleret N., Scheuerlein C., Taborelli M., (2000), *The Secondary Electron Yield of Technical Materials and its Variation with Surface Treatments*, Proceedings of EPAC 2000, Vienna, Austria, pp. 217-221

Becerra G. E. (2007), *Studies of Coaxial Multipactor in the Presence of a Magnetic Field*, U.S. Department of Energy Report, Plasma Science and Fusion, Vol. 99, pp 26-41.

Bhag S.G. and Huseyin R.H., (2004), *Electromagnetic Field Theory Funtumentals*, 2nd edition, China Machine Press, pp. 254-255

Chojnacki E. (2000), *Simulations of a multipactor-inhibited waveguide geometry*, The American Physical Society, Accelerators and Beams, Vol. 3, No. 032001, pp. 1-5

Dayton James A. (1997), *A Review of the Suppression of Secondary Electron Emission from the Electrodes of Multistage Collectors*, NASA LRC Report, pp. 1-8

Dykes D.M, Geng R.L., Belomestnykh S., Padamsee H., Goudket P., Carter R.G., (2003), *Dynamics of Multipacting in Rectangular Coupler Waveguides and Suppression Methods*, Nuclear Instrument Methods, Vol. 508, pp.227-238

European Cooperation for Space Standardization (2003), *Multipaction Design and Test*, ESA Publications Division, pp. 39-50.

Gallagher W. J. (1979), *The Multipactor Effect*, IEEE Transactions on Nuclear Science Vol. NS 26, No. 3, pp. 4280-4282

Geng R.L. and Padamsee H.S. (1999), *Exploring Multipacting Characteristics of a Rectangular Waveguide*, Proceedings of Particle Accelerator Conference, New York, NY., Vol. 05, pp. 429

Geng R.L., Belomestnykh S., H. Padamsee, Goudket P., Dykes D.M., Carter R.G. (2004), *Studies of Electron Multipacting in CESR Type Rectangular Waveguide Couplers*. Proceedings of EPAC, pp. 1057-1059

Ghatak S., Gupta N., Dhavale A. S., Mittal K.C. (2008), *Kinetic Model of Multipaction for SRF Cavities for Accelerator Driven Sub-Critical System (ADSS)*, Proceedings of EPAC08, Genoa, Italy, pp. 1741-1743

Goudket P., Bate R., Dykes D.M, Geng, R.L., Belomestnykh S., Padamsee H., R.G. Carter, (2003), *Multipacting Studies in Rectangular Waveguides*, Proceedings of EPAC, pp.1228-1230

Kishek R. A., Lau Y. Y., Ang L. K., A. Valfells, and Gilgenbach R. M., (1998) *Multipactor discharge on metals and dielectrics: Historical review and recent theories*, Physics of Plasmas, Vol. 5, pp. 2120-2126

Kumar Prashanth (2006), *Characterization of the Dose Effect in Secondary Electron Emission*, University of Madras thesis, pp 23-24.

Primdahl K., Kustom R., Maj J. (1992), *Reduction of Multipactor in RF Ceramic Windows Using a Simple Titanium-Vapor Deposition System*, U.S. Department of Energy, Office of Basic Energy Sciences Report, Vol. 31, No.109, pp 1- 3.

Proch D., Einfeld D., Onken R., Steinhauser N. (1996), *Measurement of Multipacting Currents of Metal Surfaces in RF Fields*, Elektronen-Synchrotron DESY report, pp 1-3.

Sears F.W, Zemansky M. W. and Young H.D., (1991), College Physics 6th edition, Addison Wesley publishers, Appendix A 3.2 – A 3.8

Stupakov G. and Pivi M. (2004), *Suppression of the Effective Secondary Emission Yield for a Grooved Metal Surface*, Linear Collider Collaboration Tech Notes, Vol. 0145, pp. 1-4

Valfells A, Ang L. K., Lau Y. Y., and Gilgenbach R. M. (2000), *Effects of an external magnetic field and of oblique radio-frequency electric fields on multipactor discharge on a dielectric*, Physical of Plasmas, Vol 7. No 2, pp 750-757.

Wachowski H.M. (1964), *Breakdown in Waveguides due to the Multipactor Effect*, El Segundo Technical Report, Vol. 64 N0. 77, pp 1-3.

APPENDIX A

Matlab Simulation Program

```
clc;

sec0=1;
Emax0=300;
ks=1;
iD=10;

ig=90*rand(1)

i=iD-iE
```

```
if i<0
    i=i*-1;
end


%Computation of Secondary emission yield at E=Ei for incident angle
i1_in_radians=pi*i/180;
sec_max1=sec0*(1+((ks.*(i1_in_radians).^2)/(2*pi)));
Emax1=Emax0*(1+((ks.*(i1_in_radians).^2)/(pi)));

%Inputs as array of values
Ei=0:1:5000;

w=Ei./Emax1;

if w<1
    k=0.62
else
    k=0.26
end

sec1=sec_max1*(w.*(exp(1-w))).^k;

%Computation of Secondary Emission Yield at E=Ei for incident projection
%angle alpha
i2_in_radians=pi*i2/180;
sec_max2=sec0*(1+((ks.*(i2_in_radians).^2)/(2*pi)));
Emax2=Emax0*(1+((ks.*(i2_in_radians).^2)/(pi)));


w=Ei./Emax2;

if w<1
    k=0.62;
else
    k=0.26;
end

sec2=sec_max2*(w.*(exp(1-w))).^k;

%Plot curve of sec1 and sec2 versus Ei
plot(Ei,sec1,'k-',Ei,sec2,'k-.');

%Label plot
xlabel('Ei, Primary Impact Energy');
ylabel('Secondary Electron Yield, SEY');
title(sprintf('GRAPH OF SECONDARY EMISSION YIELD OF IMPACT WEAPON USING
MODELLED EQUATION'));
legend('Impact with suppression','Impact without suppression');
h = get(gca,'Title');
set(h,'FontSize',8);
grid;
```